Influence of the w/c ratio on the hydration process of a magnesium phosphate cement and on its retardation by boric acid

Hugo Lahalle, Céline Cau Dit Coumes, Cyrille Mercier, David Lambertin, Céline Cannes, Sylvie Delpech, sandrine Gauffinet

Influence of the w/c ratio on the hydration process of a magnesium phosphate cement and on its retardation by boric acid

Hugo Lahalle[a], Céline Cau Dit Coumes[a,*], Cyrille Mercier[b], David Lambertin[a], Céline Cannes[c], Sylvie Delpech[c], Sandrine Gauffinet[d]

[a] CEA, DEN, DE2D, SEAD, F-30207 Bagnols-sur-Cèze cedex, France
[b] Laboratoire des Matériaux Céramiques et Procédés Associés (LMCPA), Université de Valenciennes et du Hainaut-Cambrésis, 59600 Maubeuge, France
[c] Institut de Physique Nucléaire, CNRS, Université Paris-Sud 11, 91406 Orsay Cedex, France
[d] Laboratoire Interdisciplinaire Carnot de Bourgogne, UMR6303, CNRS, Univ. Bourgogne/Franche-Comté, Faculté des Sciences Mirande, 9 Avenue Alain Savary, BP 47870, 21078 Dijon cedex, France

A B S T R A C T

Magnesium potassium phosphate cements (MKPCs) are prepared using calcined magnesia (MgO) and an acidic solution of potassium dihydrogen phosphate (KH_2PO_4). Their fast setting and high heat of hydration can be problematic when large volumes of materials are produced. Boric acid ($B(OH)_3$) is thus commonly added as a set retarder. This work investigates MKPC hydration in paste (water-to-cement ratio w/c = 1) and its retardation by $B(OH)_3$. The precipitation of K-struvite ($MgKPO_4{\cdot}6H_2O$) is preceded by that of phosphorösslerite ($MgHPO_4{\cdot}7H_2O$) and $Mg_2KH(PO_4)_2{\cdot}15H_2O$. Cattiite ($Mg_3(PO_4)_2{\cdot}22H_2O$), an end-product in diluted suspension (w/c = 100), is not observed. $B(OH)_3$ slows down the formation of hydrates in two ways: (*i*) by stabilizing in solution the cations that outbalance the negative charges of the polyborates formed at pH above 6, and (*ii*) through the precipitation of an amorphous mineral containing borate and orthophosphate. The first process occurs both in diluted suspensions and pastes, the second is specific to pastes.

Keywords:
A: hydration
A: retardation
B: hydration products
D: MgO
D: chemically-bonded ceramics

1. Introduction

Magnesium phosphate cements (MPCs) are clinker-free binders, referred to as acid-base cements since they are prepared by mixing an acidic water-soluble phosphate salt with a weakly basic magnesium oxide calcined at high temperature to decrease its reactivity [1,2]. They are mainly used as mortar or concrete for rapid repairs [3–5]. They set and harden fast, they have good volume stability, and they bond well to mature concrete based on Portland cement. MPCs have also attracted interest for biomedical application due to their antibacterial activity and biocompatibility [6–8]. Besides, they offer new prospects for the stabilization/solidification of hazardous waste, such as heavy metals [9–15], grinding dusts [16] and radioactive waste [17–22].

When ammonium phosphate salts (such as $(NH_4)_2HPO_4$ or $(NH_4)H_2PO_4$) are used to prepare MPCs, the main product formed is struvite ($Mg(NH_4)PO_4{\cdot}6H_2O$) [23]. Noxious ammonia can however be released during the setting and hardening process. This drawback can be avoided by replacing the ammonium salt by a sodium or potassium salt [1,2,6,24]. Potassium salts tend to be preferred since they yield more crystalline hydrated phases and mechanically stronger materials as long as the Mg/P molar ratio is < 8 [25]. The major hydration product is then K-struvite ($MgKPO_4{\cdot}6H_2O$).

$$MgO + KH_2PO_4 + 5\,H_2O \rightarrow MgKPO_4{\cdot}6H_2O \quad (1)$$

In most materials based on magnesium potassium phosphate cements (MKPC), MgO is introduced in excess with respect to KH_2PO_4 (MgO/KH_2PO_4 molar ratio (Mg/P) > 1) because this limits the risk of efflorescence, increases the final mechanical strength and reduces the drying shrinkage [26–29]. Many studies have shown indeed that, at a given water-to-cement ratio (w/c, where c stands for the mass of MgO and KH_2PO_4), the final strength of a hardened cement paste increases with the Mg/P molar ratio, reaches a maximum (for Mg/P ratios typically within the range 3–6, the optimal value depending on the w/c ratio), and then decreases [30–34]. In the context of radioactive waste management, MKPCs can be used to stabilize and solidify hazardous waste that interacts adversely with conventional Portland-cement based materials [17–22]. There are questions however regarding the long-term evolution in the humid environments of repositories of MKPC-based materials containing unreacted MgO [35]: it is well known that the hydration of MgO into $Mg(OH)_2$ is accompanied by a significant

(118%) increase in volume which can lead to substantial expansion in hardened cement-based materials [36,37]. This is the reason why, for instance, the maximum MgO content in standardized cements is limited to 5 wt% in Europe (standard EN 197-1). Given this uncertainty about the long-term evolution of MKPC-based materials with MgO in excess over KH_2PO_4, the Mg/P molar ratio of the MKPCs investigated in this study was set to 1. Besides, this low Mg/P molar ratio provides another benefit for the encapsulation of waste which is unstable in alkaline media: the pore solution pH of hydrated MKPC is close to 8 [21], instead of > 10 for hydrated MKPCs with higher Mg/P molar ratios [38,39].

The hydration process of MKPC is more complex than suggested by the mass balance equation (Eq. (1)). It involves several steps, but the exact number of steps and the nature of the transient products remain debated. Chau et al. [40] investigated cement suspensions with Mg/P ratios between 4 and 12 and a w/c ratio of 10. They showed that the precipitation of K-struvite at pHs above 7 was preceded by that of $MgHPO_4{\cdot}7H_2O$ (phosphorösslerite) in acidic solution (pH ~ 4), and by that of $Mg_2KH(PO_4)_2{\cdot}15H_2O$ at intermediate pHs. A similar sequence was also observed by Zhen et al. [41] in cement pastes (Mg/*P* = 5, w/c = 0.1) retarded by heavy metals (Cu, Ni, Zn and Cd), and by us in cement suspensions (w/c = 100) with a lower Mg/P ratio (Mg/*P* = 1) [42]. However, two recent studies have reported different results. Viani et al. [43] investigated the hydration of cement pastes (Mg/P = 1, w/c = 0.3) using in situ synchrotron powder diffraction and concluded that hydration involved two consecutive, partly overlapping processes. The precursor of K-struvite, which was amorphous or poorly crystalline, was not identified however. Le Rouzic et al. [44] also investigated cements with equimolar amounts of MgO and KH_2PO_4 (Mg/*P* = 1) in pastes (w/c = 0.2) or suspensions (w/c = 3.86) and reported in both cases that newberyite ($MgHPO_4{\cdot}3H_2O$) precipitated before K-struvite.

MKPCs are highly reactive and their hydration is exothermic. When large volumes of material are prepared, an autocatalytic process takes place: the heating accelerates the reactions, so that the material can set almost instantaneously. MKPC binders thus need to be retarded for field applications. The most commonly used retarders are boric acid and sodium borate [45–47], but their mechanisms of action are not fully understood. There are two main hypotheses. The dissolution of MgO may be slowed down either by the adsorption of $B(OH)_3$ [48] or by the precipitation of a coating layer of a borate-containing mineral (well crystallized lünebergite $Mg_3B_2(PO_4)_2(OH)_6{\cdot}6H_2O$ [49,50], or an amorphous or poorly crystalline unidentified compound [51]). Alternatively, aqueous magnesium might be stabilized in solution by the formation of a magnesium borate complex [50]. In a previous study devoted to the hydration of MKPC (Mg/*P* = 1) in a diluted suspension (w/c = 100) [42], we confirmed the retarding effect of boric acid under these conditions and showed that boron did not precipitate, but remained dissolved in the solution. It had no influence on the initial dissolution of the reactants (MgO and KH_2PO_4), but retarded the precipitation of the products. It also changed the phase assemblage. In a basic medium, boric acid was found to dissociate into anionic forms ($B(OH)_4^-$ and polyborates at high boron concentration). These negative charges were balanced by an increase in the aqueous concentration of potassium, which promoted the precipitation of cattiite ($Mg_3(PO_4)_2{\cdot}22H_2O$) instead of K-struvite. Under the conditions of the study, the $MgB(OH)_4^+$ complex was present in too small amounts to play a key role in the retardation process.

Investigating cement hydration in diluted suspension has several advantages. Analyzing the aqueous phase is easier, and the duration of the different stages of hydration is increased, which is very helpful to characterize fast reacting systems. However, if the dilution factor is too large, the solution may remain undersaturated with respect to the minerals that would precipitate in pastes, and the hydration process is modified. To better understand the influence of the w/c ratio on the hydration process of MKPC and on the retardation by boric acid, this paper complements our previous work devoted to diluted suspensions (w/c = 100) [42] by investigating MKPC pastes with a much lower water content (w/c = 1).

2. Experimental

2.1. Preparation of cement pastes

MKPC pastes were prepared using hardburnt magnesia (MgO MAGCHEM 10 CR from M.A.F. Magnesite BV; particle size distribution: d_{10} = 4.8 µm, d_{50} = 18.9 µm, d_{90} = 45.6 µm; specific surface area ≈ 0.9 m^2/g; chemical composition (wt%): MgO (98.3), CaO (0.90), SiO_2 (0.40), Fe_2O_3 (0.20), Al_2O_3 (0.10), Cl (0.01), SO_3 (0.01), loss on ignition (0.25)), potassium dihydrogen phosphate (KH_2PO_4) (VWR, purity > 98%, d_{10} = 175 µm, d_{50} = 365 µm, d_{90} = 594 µm) and deionized water.

Five cement pastes were investigated. The Mg/P molar ratio was set to 1, as was the w/c weight ratio. This high water content was selected for two reasons. First, it is above the chemical water demand of the cement (corresponding to a w/c ratio of 0.51 according to Eq. (1)). Second, the volume of pore solution extracted from the paste samples after increasing periods of hydration was sufficient to be analyzed. To avoid bleeding and to obtain homogeneous materials, the cement pastes were kept under magnetic stirring (200 r.p.m) until they set. Boric acid was added to the mixing solution at different concentrations: 0, 4.17, 41.7, 208 and 417 mmol/L. The latter corresponds to a boric acid-to-cement ratio of 2.58 wt%, which is typical for MKPC pastes and mortars [21,46,52]. The different paste samples were subsequently labelled P_x, with *x* standing for their boric acid content (in wt% with respect to cement). The contents of the different mixtures are summarized in Table 1.

Potassium dihydrogen phosphate and boric acid (if any) were first added to 250 g of demineralized water. Dissolution was complete for boric acid, but only partial for KH_2PO_4 since its concentration exceeded its solubility limit (25 g in 100 mL water at 25 °C [53]). The endothermic dissolution of KH_2PO_4 caused a decrease in the temperature of the suspension which was therefore kept under stirring for approximately 1 h in a thermostatic bath at 25 °C. Once the temperature had stabilized again at 25 °C, the MgO powder was added and the mixture was stirred for 3 min using a mechanical stirrer.

2.2. Characterization of specimens

The hydration of the cement pastes was characterized using a CAD Instruments Multicad CDM 210 conductivity meter. The conductimetric cell was cylindrical (inner radius of 15 mm, total volume of 70 mL) and comprised two annular stainless steel electrodes (a sketch of the setup is

Table 1
Composition of MKPC pastes (for 250 g of water).

Paste reference	Water/cement wt. ratio	Mg/P molar ratio	MgO (g)	KH_2PO_4 (g)	$B(OH)_3$ (g)	$[B(OH)_3]$ (mmol/L)	$B(OH)_3$/cement ratio (wt%)
$\#P_0$	1	1	57.25	192.75	0	0	0
$\#P_{0.03}$	1	1	57.25	192.75	0.06	4.17	0.03
$\#P_{0.26}$	1	1	57.25	192.75	0.64	41.7	0.26
$\#P_{0.67}$	1	1	57.25	192.75	1.67	108	0.67
$\#P_{2.58}$	1	1	57.25	192.75	6.44	417	2.58

Table 2
Details of the synthesis of reference magnesium phosphate minerals.

Mineral	Reactants	Duration of reaction	Final pH
K-struvite ($MgKPO_4{\cdot}6H_2O$)	11.57 g KH_2PO_4 (85 mmol) 3.43 g MgO (85 mmol) 150 mL demineralized water	30 h	8.0
Newberyite ($MgHPO_4{\cdot}3H_2O$)	11.57 g KH_2PO_4 (85 mmol) 16.16 g $MgCl_2.6H_2O$ (79.5 mmol) 150 mL demineralized water	7 d	6.8
Cattiite ($Mg_3(PO_4)_2{\cdot}22H_2O$)	575 µL H_3PO_4 (at 14.83 mol/L) (8.5 mmol) 28.24 g $MgCl_2.6H_2O$ (138.9 mmol) 0.42 g LiOH 150 mL demineralized water	3 d	6.5
$Mg_2KH(PO_4)_2{\cdot}15H_2O$	6.92 g K_2HPO_4 (39.8 mmol) 9.80 g $MgSO_4.7H_2O$ (39.8 mmol) 150 mL demineralized water	30 min	6.1
Phosphorösslerite + MgO ($MgHPO_4{\cdot}7H_2O$ + MgO)	11.57 g KH_2PO_4 (85 mmol) 3.43 g MgO (85 mmol) 150 mL demineralized water	30 min	6.0
Lünebergite $Mg_3B_2(PO_4)_2(OH)_6{\cdot}6H_2O$	3.87 g $B(OH)_3$ (62.6 mmol) 1.157 g KH_2PO_4 (8.5 mmol) 0.344 g MgO (8.5 mmol) 150 mL demineralized water	1 d	7.0

given in reference [54] – in the work reported here, the helicoidal ribbon blade shown in [54] was replaced by a magnetic stirring bar). It was connected to the electroconductivity channel of an electrochemistry meter. A specific data acquisition software was used to collect the conductivity measurements. The cell was thermostated at 25 °C by circulating cooling water in a double envelope. It was first calibrated using a 12.88 mS/cm standardized KCl solution at 25 °C, and then filled with the fresh paste sample under investigation which was maintained under magnetic stirring until it set. Supplementary experiments on suspensions were performed using a similar device, but with a larger thermostated cell (volume of 250 mL).

The Vicat setting time was measured according to the European standard procedure EN 196-3. The needle was placed on a 300 g moveable rod and had a diameter of 1 mm ± 0.05 mm. A sample of fresh cement paste was cast in a frustum 40 mm in height, with top and bottom internal diameters of 70 and 80 mm respectively. The initial setting time was considered to be the time when the needle penetration was 39 mm ± 0.5 mm. The final setting time corresponded to a penetration of < 0.5 mm.

After mixing, some of the paste samples were cast into airtight polypropylene boxes (≈20 g of paste per box) and cured at 25 °C. The samples were homogenized by magnetically stirring them until they set. Cement hydration was stopped after fixed periods of time, which varied between samples, by successively immersing the crushed pastes into isopropanol for 30 min and drying them in a controlled humidity chamber (with 20% relative humidity at 23 ± 2 °C).

Crystalline phases were identified by powder X-ray diffraction (XRD) with the Bragg Brentano geometry (PANalytical X'Pert PRO MPD - copper anode $\lambda_{K\alpha1}$ = 1.54056 Å generated at 45 mA and 40 kV, X'celerator detector) performed on pastes ground by hand to a particle size of < 100 µm. The XRD patterns were collected in the 2θ range 5–70° with 0.017° steps, corresponding to 0.625 s measurement time per step. Thermogravimetric analyses (TGAs) were carried out using a TGA/DSC Netzsch STA 409 PC instrument. The samples were heated under nitrogen at 10 °C/min up to 1000 °C.

^{31}P and ^{11}B solid state NMR analyses were also carried out to complete the characterization of the solids and determine the evolution of the crystalline and amorphous phases over time. The ^{31}P NMR spectra were collected on a Bruker Avance I 400 MHz spectrometer (9.4 T, ^{31}P Larmor frequency, 162 MHz) using a probe for 4 mm o.d. zirconia rotors, a magic angle spinning (MAS) frequency of 12.5 kHz, 2 µs (25°) pulses, and proton decoupling at 70 kHz during the acquisition period. A minimum of 8 scans were coadded and the relaxation delay was 300 or 600 s depending on the sample. The spectra were referenced to H_3PO_4 (85% solution). The ^{11}B NMR spectra were collected on a Bruker Avance I 800 MHz spectrometer (18.8 T, ^{11}B Larmor frequency, 256.7 MHz) using a probe for 3.2 mm o.d. zirconia rotors, a MAS frequency of 12.5 kHz and 1 µs (18°) pulses. A minimum of 128 scans were coadded and the relaxation delay was 5 s. The spectra were referenced to $NaBH_4$. All the NMR spectra were analyzed using the software DMFit [55].

Two-dimensional ^{11}B - ^{31}P NMR correlations experiments were carried out on a Bruker Avance I 800 MHz spectrometer (18.8 T, Larmor frequencies of 256.8 and 324.1 MHz for ^{11}B and ^{31}P, respectively) using a probe for 3.2 mm o.d. zirconia rotors and a MAS frequency of 20 kHz. One dimensional ^{11}B MAS NMR spectra were recorded using 1 µs (10°) pulses and 128 to 4096 scans were coadded with a relaxation delay of 2 s. One-dimensional ^{31}P MAS NMR spectra were recorded using 4 µs (90°) pulses and 8 scans were coadded with a relaxation delay of 120 s. $^{31}P/^{11}B$ dipolar correlation maps were acquired at 18.8 T using a ^{11}B (^{31}P)D-HMQC [56,57] pulse sequence and a homemade $^{11}B/^{31}P$ probe for 3.2 mm o.d. zirconia rotors. A total of 1236 × 24 points were recorded with 160 scans and a relaxation delay of 2 s, with 10 and 4 µs pulses (90° tip angle) on the ^{11}B and ^{31}P channels respectively, and a 2 ms recoupling time with the SR421 pulse sequence [58]. According to Tricot et al. [59], the B/P spatial proximities identified using short recoupling times such as this can be assumed to indicate the presence of chemical bonds.

During the first stages of hydration (up to 40 h), the pore solution of the cement pastes was also extracted by compaction of ~20 g samples with a Carver mechanical press at a pressure of 34 MPa. The pH of the recovered liquid was immediately measured with a pH electrode (Mettler Toledo InLab Expert Pt1000 pH 0–14 T 0–100 °C) calibrated using two IUPAC pH buffers at 4.01 (25 °C) and 9.18 (25 °C). 1 mL aliquots were sampled using a syringe, filtered at 0.2 µm, and diluted with a 2 wt% HNO_3 solution before ICP-AES analysis (Vista Pro Varian, standardization with matrix reconstitution). The experimental error was ± 5%.

2.3. Synthesis of reference phases

A set of magnesium phosphate minerals was synthesized by precipitation (Table 2) to record reference ^{31}P NMR spectra. The MgO, KH_2PO_4 and $B(OH)_3$ used were the same as for the preparation of the cement pastes. Analytical grade $MgCl_2{\cdot}6H_2O$, $MgSO_4{\cdot}7H_2O$ and H_3PO_4 85% were purchased from VWR. The reactants were added to 150 mL of

demineralized water in 250 mL reactors under magnetic stirring (500 r.p.m). The reactors were closed to prevent evaporation and were kept under stirring at room temperature for a period ranging from 30 min to 7 days. At the end of the experiments, the suspensions were filtered under vacuum. The solids were rinsed with isopropanol and dried in a controlled humidity chamber (with 20% relative humidity at 23 ± 2 °C) before being characterized by XRD and MAS NMR (^{31}P, and ^{11}B for lünebergite). The XRD patterns (shown in the Appendix A) confirmed the presence of pure crystalline phases, except for phos-phorösslerite ($MgHPO_4{\cdot}7H_2O$) which was mixed with residual MgO, and $Mg_2KH(PO_4)_2{\cdot}15H_2O$ which contained possible traces of K-struvite (diffraction peak at 2θ = 20.9°).

3. Results and discussion

3.1. Investigation of the hydration process of MKPC in pure water (paste #P0)

3.1.1. Electrical conductivity

The evolution of the electrical conductivity of a cement paste gives information on the different stages of its hydration process [60]. Conductivity usually increases rapidly immediately after mixing due to the dissolution of anhydrous cement phases. The solution then becomes oversaturated with respect to the cement hydrates which precipitate. The consumption of ions and the decrease in their mobility due to the progressive structuring of the paste lead to a conductivity decrease which is sharp when there is a massive precipitation of hydrates.

As observed previously with diluted cement suspensions [42], the electrical conductivity of paste $\#P_0$ evolved non monotonously over time, with a profile typical of a multi-step process (Fig. 1-a). The electrical conductivity increased rapidly when MgO started to dissolve, levelled off after 15 min, and increased again to reach a maximum at 30 min (Fig. 1-b). It then decreased in two stages. The final set occurred at 45 min, during the first drop in conductivity.

3.1.2. Solid phase evolution

3.1.2.1. Characterization by XRD and TGA. The phase assemblage of paste $\#P_0$ was characterized by XRD and TGA during the first day of hydration (Fig. 2, Fig. 3). KH_2PO_4 was consumed much faster than MgO: the former was almost fully exhausted after 15 min, whereas traces of the latter were still observed at 24 h. K-struvite was detected by XRD from 30 min onwards. The thermograms also exhibited a weight loss at 120 °C due to the dehydration of this phase [61]. The two transient products previously observed in diluted suspensions [42](phosphorösslerite ($MgHPO_4{\cdot}7H_2O$) and $Mg_2KH(PO_4)_2{\cdot}15H_2O$) also precipitated in the paste. They were detected by XRD from 30 min until 1 h and until 1 h 15 min respectively. The presence of $Mg_2KH(PO_4)_2{\cdot}15H_2O$ was also detected by TGA through its contribution to the weight loss event below 100 °C [42]. There is still some uncertainty concerning the dehydration temperatures of phosphorösslerite ($MgHPO_4{\cdot}7H_2O$). This mineral is well-known to be highly unstable however. It rapidly converts into newberyite ($MgHPO_4{\cdot}3H_2O$), even at room temperature [62,63]. One can therefore assume that phosphorösslerite started to dehydrate below 100 °C to form newberyite. The small weight loss event at 180 °C corresponded to the dehydration of newberyite, in agreement with previously reported data [64]. Other minerals may also have formed transiently: the weak diffraction lines at 2θ = 22.1°, 23.1° and 24.7° in the patterns recorded at 45 min and 1 h could not be assigned.

3.1.2.2. Characterization by ^{31}P MAS-NMR spectroscopy. Prior to the characterization of paste $\#P_0$ by ^{31}P MAS NMR, some reference spectra were recorded of KH_2PO_4 and the synthesized magnesium phosphate hydrates (Fig. 4). The chemical shifts measured for KH_2PO_4 (δ = 3.9 ± 0.1 ppm), K-struvite (δ = 6.4 ± 0.1 ppm) and newberyite (δ = −7.5 ± 0.1 ppm) are within a few tenths of a ppm of those reported in the literature for these hydrates (3.6 ppm [52], 6.2 ppm [52] and − 7.2 ppm [65] respectively). In contrast, the chemical shift measured for cattiite (δ = 6.9 ± 0.1 ppm) was markedly different from the one mentioned by Aramendia et al. [66] (δ = 1.1 ± 0.1 ppm, spectrum not shown in the paper). The spectrum of K-struvite contains a weak shoulder at δ = 5.7 ppm, indicating the presence of trace amounts of another phase for which there are at least two possible assignments. Kovdorskite ($Mg_2PO_4(OH){\cdot}3H_2O$) has a chemical shift close to 5 ppm and is observed in small amounts in MPC cement pastes containing struvite ($Mg(NH_4)PO_4{\cdot}6H_2O$) [67]. A $Mg_3(PO_4)_2{\cdot}xH_2O$-type phase might also be formed in small amounts, as already observed in diluted suspensions [42]. The spectra of phosphorösslerite ($MgHPO_4{\cdot}7H_2O$) and $Mg_2KH(PO_4)_2{\cdot}15H_2O$ are reported here for the first time. The width of the peak from $Mg_2KH(PO_4)_2{\cdot}15H_2O$ suggests that it is of low crystallinity (the compound was nonetheless detected by XRD) or that other amorphous minerals are present alongside well-crystallized $Mg_2KH(PO_4)_2{\cdot}15H_2O$. This second hypothesis is supported by the following observation: simulating the $Mg_2KH(PO_4)_2{\cdot}15H_2O$ peak required four components with chemical shifts at 2.6, 3.1, 3.4 and 3.7 ppm (Fig. 4), which suggests that the phosphorus atoms are in four different chemical environments. However, the crystallographic structure of $Mg_2KH(PO_4)_2{\cdot}15H_2O$ established by Takagi et al. [68] contains only one type of phosphorus site.

The ^{31}P MAS-NMR spectra recorded for paste $\#P_0$ during the hydration period are shown in Fig. 5. At 15 min, the only phosphate mineral present was KH_2PO_4. This reactant was detected until 1 h. The phosphorösslerite ($MgHPO_4{\cdot}7H_2O$) peak was observed from 30 min to

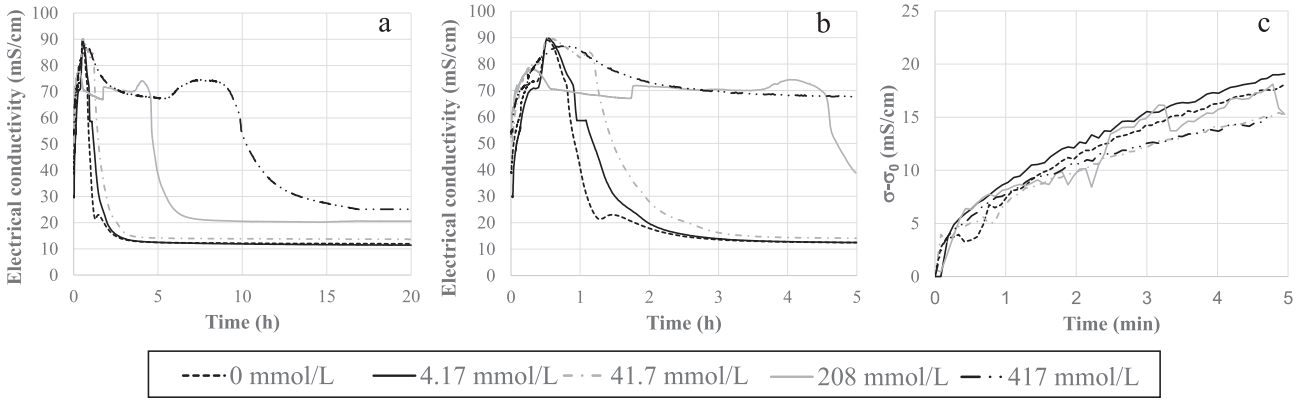

Fig. 1. Influence of the initial concentration of boric acid on the electrical conductivity of pastes $\#P_0$, $\#P_{0.03}$, $\#P_{0.26}$, $\#P_{0.67}$ and $\#P_{2.58}$ (w/c = 1, Mg/P = 1, $[B(OH)_3]$ varying from 0 to 417 mmol/L). ($\sigma-\sigma_0$) represents the electrical conductivity, corrected from its initial value before the addition of MgO. (b) and (c): expanded views respectively of the first 5 h and the first 5 min.

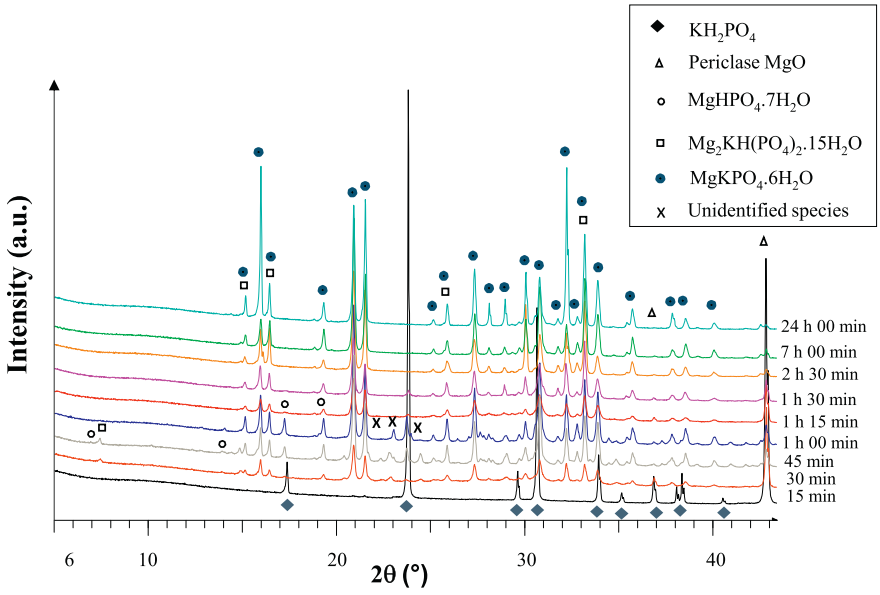

Fig. 2. X-ray diffraction patterns of the solid fraction of paste #P_0 comprising MgO, KH_2PO_4 and H_2O (w/c = 1, Mg/*P* = 1) at different stages of hydration.

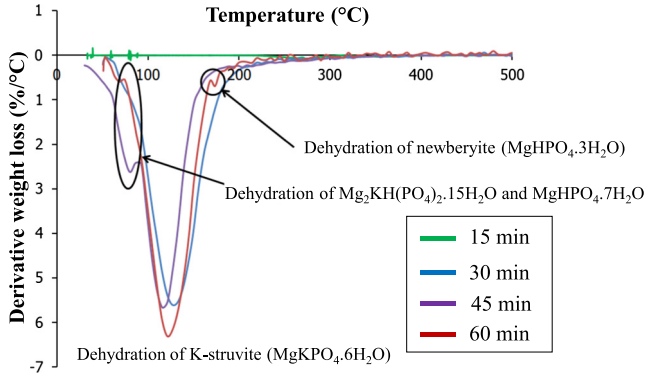

Fig. 3. Thermogravimetric analysis of the solid fraction of paste #P_0 comprising MgO, KH_2PO_4 and H_2O (w/c = 1, Mg/P = 1) during the early stages of hydration (from 15 min to 1 h).

2 h 30 min. NMR spectroscopy was thus more sensitive than XRD for which the concentrations of KH_2PO_4 and $MgHPO_4{\cdot}7H_2O$ fell below the detection limit after 15 min and 1 h 15 min respectively. The $Mg_2KH(PO_4)_2{\cdot}15H_2O$ peak appears in the spectra recorded from 30 min to 1 h, and possibly in the one recorded after 7 h, but in a much less crystalline state given the linewidth observed. K-struvite ($MgKPO_4{\cdot}6H_2O$) started to precipitate from 30 min onwards and was the main product detected by NMR in the 7 h- and 16 h-old pastes. Traces of newberyite ($MgHPO_4{\cdot}3H_2O$) were detected at all measurement times except the first. Limited access to the spectrometer meant that the NMR spectra of the paste samples were recorded at least 2 weeks after the hydration stop. This delay was long enough to cause significant dehydration of phosphorösslerite ($MgHPO_4{\cdot}7H_2O$) into newberyite ($MgHPO_4{\cdot}3H_2O$), as shown by the two XRD patterns in Fig. 6, recorded on a 30-min old sample just after the hydration stop and two weeks later. In between, the sample had been stored in an air-tight polypropylene container (volume = 30 mL) at room temperature (23 ± 2 °C) and was not protected from light. This observation is consistent with the work of Kiehl et al. [62] who found that $MgHPO_4.7H_2O$ converted into $MgHPO_4{\cdot}3H_2O$ in a day or two when the freshly synthesized crystals were stored in a glass-stoppered bottle at ambient temperature, or in a week when the crystals were kept in the solution from which they had precipitated. The NMR spectra of the samples after 30 min, 45 min and 1 h of hydration contain a peak at δ = 5.3 ppm from an unidentified phase which may also have been responsible for the unassigned reflections at 2θ = 22.1°, 23.1° and 24.7° in the XRD patterns (Fig. 2). At the end of the hydration period, a weak peak was also observed at a chemical shift of 4.6 ppm. This might come from bobierrite ($Mg_3(PO_4)_2{\cdot}8H_2O$) which is known to have a chemical shift between 4.0 and 4.6 ppm [64,66].

3.1.3. *Liquid phase evolution*

Fig. 7 shows the chemical composition of the pore solution

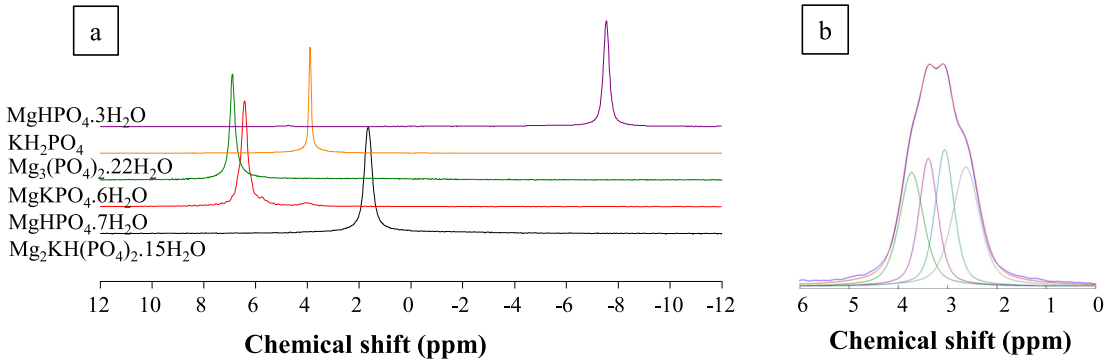

Fig. 4. ^{31}P MAS-NMR spectra of KH_2PO_4 and five synthesized magnesium phosphate hydrates (a). Fit using four components of the ^{31}P spectrum of $Mg_2KH(PO_4)_2{\cdot}15H_2O$ (b).

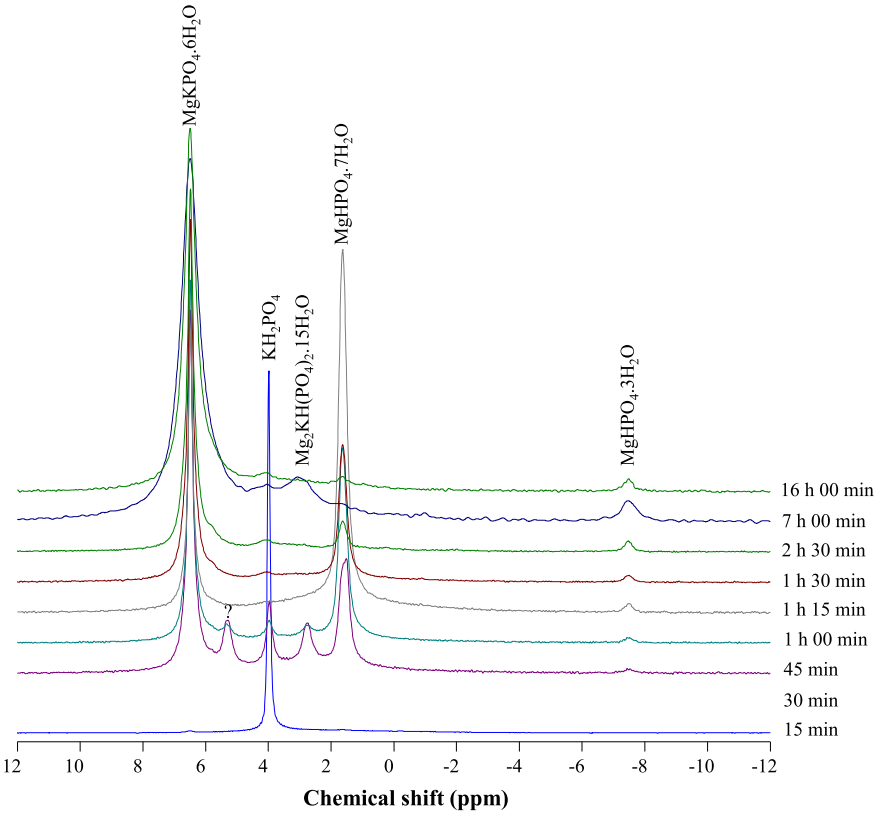

Fig. 5. ^{31}P MAS NMR spectra of the solid fraction of paste #P_0 comprising MgO, KH_2PO_4 and H_2O (w/c = 1, Mg/*P* = 1) at different stages of hydration (from 15 min to 16 h).

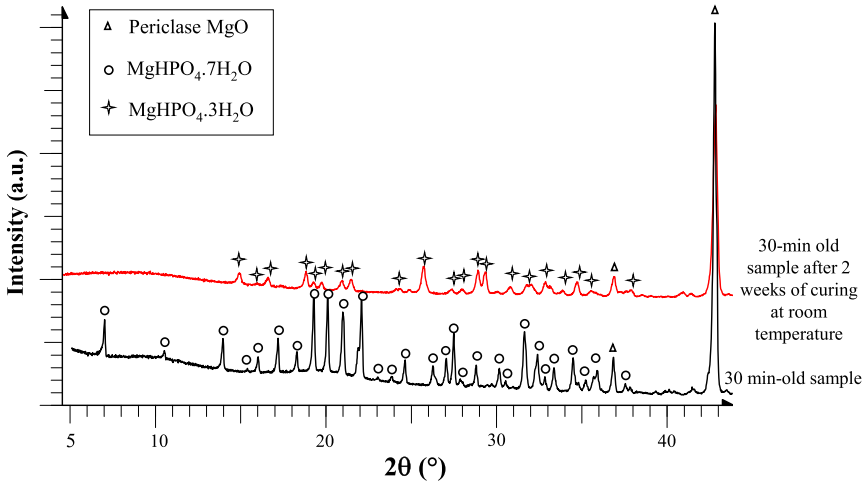

Fig. 6. XRD patterns of the solid fraction of a cement suspension comprising MgO, KH_2PO_4 and H_2O (w/c = 10, Mg/P = 1) after 30 min. The measurements were performed immediately after the hydration stop (black line), or 2 weeks later (red line, the sample was stored between the two analyses at ambient temperature in an air-tight polypropylene container). (For interpretation of the references to colour in this figure legend, the reader is referred to the web version of this article.)

extracted from paste #P_0 after increasing periods of hydration. The different identifiable stages are as follows. (*i*) From 0 to 15 min, the dissolution of MgO (Eq. (2)) leads to an increase in the Mg concentration (from 0 to 1313 mmol/L) and the pH (from 4.4 to 6.5).

$$MgO + 2\,H^+ \rightarrow Mg^{2+} + H_2O \quad (2)$$

This increase in pH increases the solubility of KH_2PO_4. Therefore, the K and P concentrations also increase.

(*ii*) From 20 min to 40 min, the pH keeps on increasing from 6.5 to 7.4. The P concentration starts to decrease, whereas the K concentration remains approximatively constant. This is consistent with the precipitation of phosphorösslerite ($MgHPO_4{\cdot}7H_2O$), a potassium-free magnesium phosphate hydrate, observed by XRD, NMR and TGA. However, the NMR data also suggest that small amounts of $Mg_2KH(PO_4)_2{\cdot}15H_2O$ and $MgKPO_4{\cdot}6H_2O$ precipitated. A plausible interpretation is then that the consumption of potassium in these reactions was counterbalanced by two processes: a release of potassium into the solution from the dissolution of KH_2PO_4, and the decrease in the water content due to the ongoing hydration (thus, maintaining a constant K concentration overall).

(*iii*) From 45 min to 1 h, the pH slightly increases from 7.4 to 7.7 while the P and K concentrations decrease simultaneously. The rates at which K and P are consumed in forming the hydrates ($Mg_2KH(PO_4)_2{\cdot}15H_2O$, $MgHPO_4{\cdot}7H_2O$ and $MgKPO_4{\cdot}6H_2O$ as shown by the solid-state analysis) thus exceed the rate at which KH_2PO_4 dissolves.

(*iv*) From 1 h to 1.5 h, the pH increases from 7.7 to 8.2, the K and P concentrations increase transiently, and the Mg concentration decreases

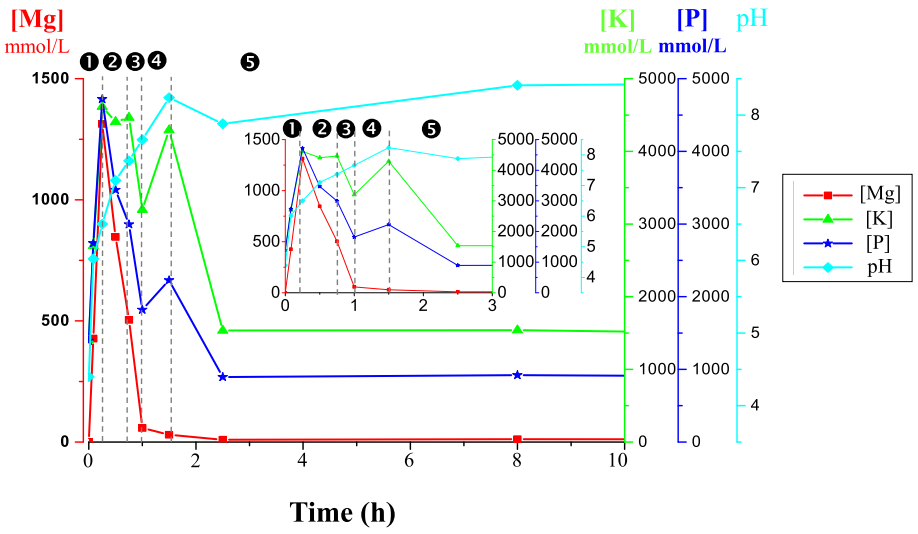

Fig. 7. Chemical composition and pH of the pore solution of paste #P_0 during hydration (w/c = 1, Mg/*P* = 1, $[B(OH)_3]$ = 0 mmol/L – the inset shows an expanded view of the data for the first 3 h).

slightly. The XRD and NMR data show that $Mg_2KH(PO_4)_2{\cdot}15H_2O$ dissolves during this period. However, the potassium concentration increases more than the phosphate concentration does, which is inconsistent with the stoichiometry of $Mg_2KH(PO_4)_2{\cdot}15H_2O$. This may be because $Mg_2KH(PO_4)_2{\cdot}15H_2O$ dissolves incongruently, but a more likely explanation is that a phosphate-containing mineral precipitates, such as $MgHPO_4{\cdot}7H_2O$ whose precipitation is evidenced in the NMR data up to 1 h 15 min.

(*v*) After 1.5 h, the concentrations decrease again and level off after 2.5 h. The pH shows little change and remains between 8.2 and 8.4. The main product of hydration is K-struvite.

3.1.4. *Discussion: influence of the w/c ratio on the hydration of MKPC*

The hydration process observed here for MKPC in paste (w/c = 1) shows strong similarities with that previously described for diluted suspensions (w/c = 100) [42]:

- phosphorösslerite ($MgHPO_4{\cdot}7H_2O$) and $Mg_2KH(PO_4)_2{\cdot}15H_2O$ precipitate transiently during the first stages of hydration,
- the main final product is K-struvite ($MgKPO_4{\cdot}6H_2O$),
- newberyite ($MgHPO_4{\cdot}3H_2O$) forms as a degradation product of phosphorösslerite ($MgHPO_4{\cdot}7H_2O$) during sample storage after the hydration stop.

There are some differences however. (*i*) Other transient phases precipitate in small amounts in the paste, as suggested by the unassigned peaks in the XRD patterns and NMR spectra of the samples aged for 30 min to 1 h. (*ii*) Cattiite ($Mg_3(PO_4)_2{\cdot}22H_2O$), which forms in addition to K-struvite in diluted suspension, was not observed anymore here in the paste. Nonetheless, the ^{31}P NMR data do point toward the possible formation of trace amounts of a less hydrated magnesium phosphate hydrate (bobierrite $Mg_3(PO_4)_2{\cdot}8H_2O$). (*iii*) The final pH of the pore solution is lower in the paste than in the diluted suspension (pH 8.4 vs pH 10), which may be due to the different phase assemblages. In our previous study [42], we showed that the pHs calculated for a solution in equilibrium with either K-struvite or a mix of K-struvite and cattiite were 7.9 and 10.0 respectively.

3.2. *Investigation of the hydration process of MKPC in the presence of boric acid*

3.2.1. *Electrical conductivity*

Fig. 1 compares the electrical conductivity of cement pastes prepared with boric acid solutions of increasing concentrations. The higher the initial boric acid concentration was, the longer it took for the last drop in conductivity to occur (corresponding to a massive precipitation of hydrates and the loss of mobility of the ionic species) (Fig. 1-b), and the higher the residual conductivity was (Fig. 1-a). Boric acid does not seem to influence the different stages of hydration in the same way. A focus on the first minutes (Fig. 1-c) shows that the boric acid concentration had little influence on the initial MgO dissolution rate. A similar experiment whereby KH_2PO_4 was added to boric acid solutions at 0 to 417 mmol/L and the electrical conductivity of the suspension was monitored over time showed that the initial dissolution rate of KH_2PO_4 did not strongly depend either on the boric acid concentration (Fig. 8). However, boric acid increased the length of the subsequent stages of the hydration of MKPC. Paste #$P_{2.58}$ only set after 9 h 30 min, instead of 45 min for the reference paste #P_0 prepared with pure water. To get a better understanding of the processes causing this retardation, the phase assemblage and chemical composition of paste #$P_{2.58}$, prepared with the most concentrated boric acid solution, were characterized over time.

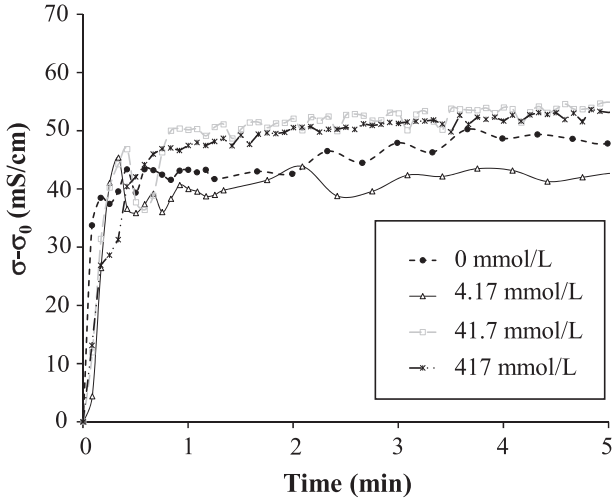

Fig. 8. Influence of the initial concentration of boric acid on the dissolution of KH_2PO_4. (σ-σ_0) represents the electrical conductivity, corrected from its initial value before the addition of KH_2PO_4 (192.75 g of KH_2PO_4 dissolved in 250 mL of a boric acid solution – same proportions as for the cement pastes).

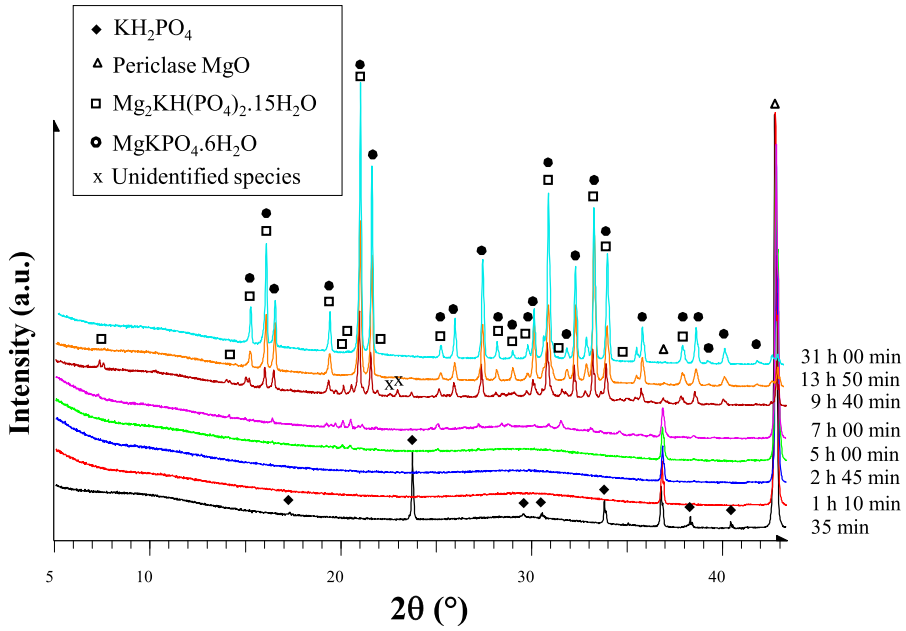

Fig. 9. X-ray diffraction patterns of the solid fraction of paste #$P_{2.58}$ comprising MgO, KH_2PO_4, $B(OH)_3$ and H_2O (w/c = 1, Mg/*P* = 1, $[B(OH)_3]_{initial}$ = 417 mmol/L) at different stages of hydration.

3.2.2. Mineralogical evolution of paste #$P_{2.58}$ ([B(OH)$_3$]$_{initial}$ = 417 mmol/L)

3.2.2.1. Characterization by XRD and TGA. The XRD patterns of paste #$P_{2.58}$ show that $Mg_2KH(PO_4)_2{\cdot}15H_2O$ and K-struvite ($MgKPO_4{\cdot}6H_2O$) precipitate as in reference paste #P_0, but after longer hydration times (Fig. 9). $Mg_2KH(PO_4)_2{\cdot}15H_2O$ was observed transiently between 7 h and 9 h 40 min (instead of between 30 min and 1 h 30 min in paste #P_0) and K-struvite was detected from 9 h 40 min onwards (instead of from 30 min for paste #P_0). The unassigned peaks at 2θ = 22.1° and 23.1°, observed for paste #P_0 at 30 min and 1 h, also appear in the diffractogram of the 9 h 40 min-old sample. No peaks corresponding to phosphorösslerite ($MgHPO_4.7H_2O$), which formed initially in paste #P_0, were observed for paste #$P_{2.58}$ however. The broad hump at 2θ ≈ 30° suggests that additional amorphous or poorly crystalline compounds precipitated during the first stages of hydration. The degradation of these compounds might explain the weight loss event below 100 °C observed in the TGA curves for the 1 h 10 min and 2 h 45 min-old samples (Fig. 10). TGA shows that K-struvite is present in all the samples investigated from 1 h 10 min to 31 h (i.e. there is weight loss for these samples at temperatures ranging from 110 to 130 °C). Only small amounts of this phase are present however until 7 h. The weight loss event at 80 °C shows that $Mg_2KH(PO_4)_2.15H_2O$ is present in the pastes aged for 7 h to 9 h 40 min, in agreement with the XRD results, but also in the 5 h-old sample.

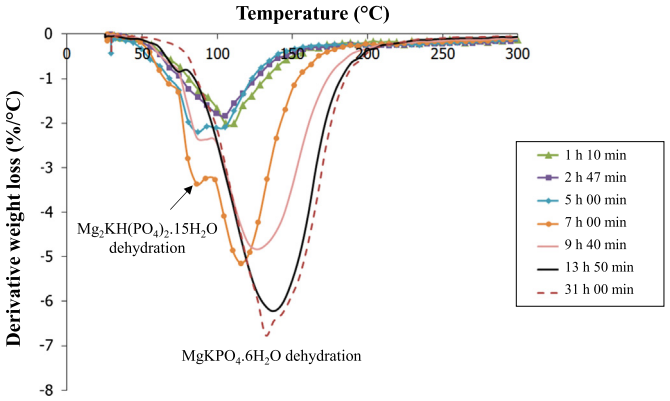

Fig. 10. Thermogravimetry analysis of the solid fraction of paste #$P_{2.58}$ comprising MgO, KH_2PO_4, $B(OH)_3$ and H_2O (w/c = 1, Mg/P = 1, $[B(OH)_3]_{initial}$ = 417 mmol/L).

3.2.2.2. Characterization by ^{31}P MAS-NMR spectroscopy. Cement paste #$P_{2.58}$ was also characterized by ^{31}P MAS-NMR spectroscopy (Fig. 11). The spectra show that residual KH_2PO_4 (δ = 3.8 ppm) was present until 7 h. This reactant was thus consumed much more slowly than in the reference paste (where it was exhausted after 1 h only). K-struvite (δ = 6.4 ppm) is present in the spectra from the first characterization time (1 h 10 min) onwards, and $Mg_2KH(PO_4)_2.15H_2O$ (δ = 2.8 ppm) from 5 h to 9 h 40 min. Because this technique is more sensitive for these materials than XRD and TGA are, small amounts of phosphorösslerite ($MgHPO_4.7H_2O$) were detected in the samples aged for 5 h and 7 h (δ = 1.7 ppm). The broad line observed from 1 h 10 min to 5 h at chemical shifts ranging from 8 to −10 ppm is clear evidence of the transient formation of an amorphous phase. This range of shifts is characteristic of orthophosphate environments in phosphate glasses [69–71].

As for reference paste #P_0, two weak peaks remained unassigned at chemical shifts of 5.1 ppm (for the samples aged for 5 h and 7 h) and 4.1 ppm (for the samples aged for 13 h 50 min and 7 d).

3.2.3. Composition of the pore solution of paste #$P_{2.58}$ ([B(OH)$_3$]$_{initial}$ = 417 mmol/L)

The pH and composition of the pore solution of paste #$P_{2.58}$ were characterized during the hydration process (Fig. 12). The pH seemed to increase in steps (from 4.1 to 6.9 between 0 h and 5 h, from 6.9 to 7.5 between 7 h and 9 h 40 min, and from 7.5 to 7.8 between 13 h 50 min and 18 h) before levelling off at 7.8. The pH increased more slowly than it did for paste #P_0 and the final value was slightly lower. Boron was partly consumed during the first 5 h of hydration. Its concentration increased however from 5 h to 18 h and levelled off afterwards. The increase in the boron concentration was accompanied by a drop in the concentrations of Mg, P and K, which then followed almost the same evolution as previously described for paste #P_0 and diluted cement suspensions [42]: (*i*) a decrease in the Mg and P concentrations from 5 h to 7.5 h due to the precipitation of several hydrates ($MgHPO_4{\cdot}7H_2O$, $Mg_2KH(PO_4)_2{\cdot}15H_2O$, $MgKPO_4.6H_2O$), the K concentration remaining

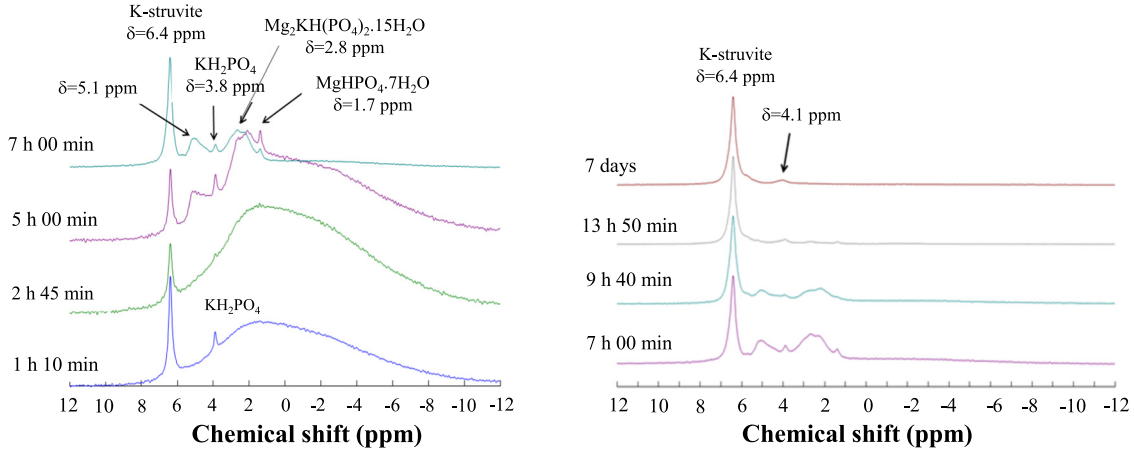

Fig. 11. ^{31}P MAS NMR spectra of the solid fraction of paste #$P_{2.58}$ comprising MgO, KH_2PO_4, $B(OH)_3$ and H_2O (w/c = 1, Mg/*P* = 1, $[B(OH)_3]_{initial}$ = 417 mmol/L) at different stages of hydration (1 h 10 min to 7 days).

approximatively constant due to the simultaneous dissolution of KH_2PO_4 and the consumption of water by hydration, (*ii*) an additional decrease in the K concentration from 7.5 h to 10 h due to the exhaustion of KH_2PO_4 and the continuing precipitation of $Mg_2KH(PO_4)_2.15H_2O$ and K-struvite (whereas $MgHPO_4.7H_2O$ dissolved), (*iii*) a transient levelling of the Mg and P concentrations from 10 h to 15 h due to the dissolution of $Mg_2KH(PO_4)_2.15H_2O$, and (*iv*) a final decrease mainly due to the precipitation of K-struvite.

The increase in the boron concentration after 5 h could reflect the dissolution of an initially precipitated borate mineral, but a simpler explanation is that water is consumed as the cement becomes hydrated. To test these two hypotheses, the volume of pore solution was estimated at the different characterization times by subtracting the volume of water bound in the cement hydrates (obtained by TGA from the weight loss at 500 °C on the thermograms) to the volume of water used for mixing. Fig. 13-a shows that the amount of boron in the pore solution decreases, reaches a minimum at 7 h, and then increases again. Thus, the increase in the boron concentration observed in Fig. 12 results not only from the consumption of water by cement hydration, but also from the partial dissolution, after 7 h, of a borate mineral formed during the first stages of hydration. Note that the massive precipitation of hydrates also occurs after 7 h, as shown by the XRD patterns in Fig. 9, and that the pH of the pore solution exhibits its second increase (Fig. 12).

Fig. 13 (b, c, d) also compares the evolution over time of the molar numbers of Mg, K and P in the pore solutions of pastes #P_0 (reference) and #$P_{2.58}$. Boric acid delays the uptake of Mg, K and P from the solution, which fits with the delayed formation of the cement hydrates observed by XRD, TGA and ^{31}P NMR.

3.2.4. Boron speciation in the solid fraction of paste #$P_{2.58}$ ([B] = 417 mmol/L)

The analysis of the pore solution of paste #$P_{2.58}$ shows there is a partial precipitation of boron at the beginning of the hydration process. However, there is no evidence of a boron-containing crystalline phase in the XRD data. This raises two questions: what is the boron speciation in the solid phase, and does the amorphous phosphate mineral identified by ^{31}P MAS-NMR during the first hours of hydration also contain boron? The solid fraction of paste #$P_{2.58}$ was therefore also characterized by one-dimensional (^{11}B) and two-dimensional (^{11}B-^{31}P) MAS-NMR spectroscopy.

3.2.4.1. ^{11}B MAS NMR spectroscopy. The ^{11}B MAS-NMR spectra of the solid fraction of paste #$P_{2.58}$ aged from 35 min to 24 h are shown in Fig. 14. Signal was detected from the first characterization time

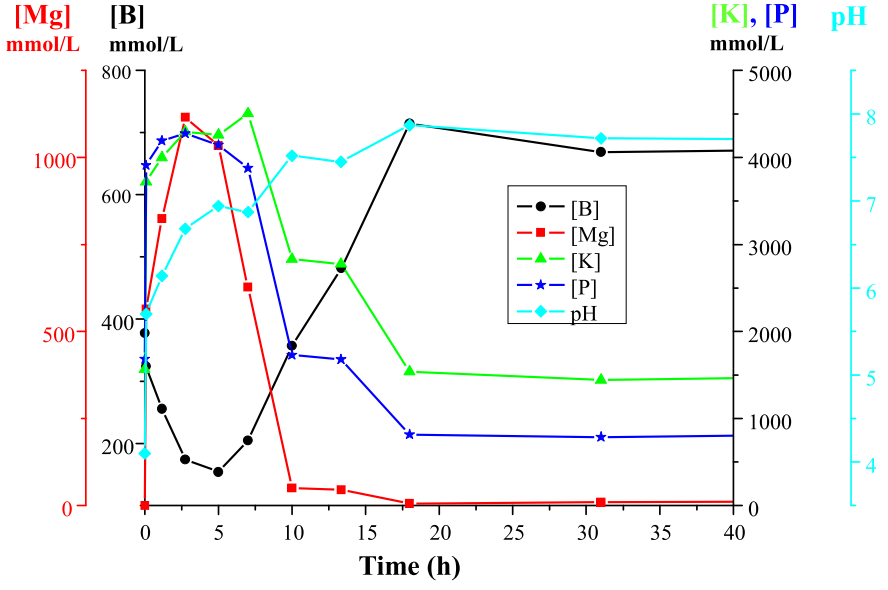

Fig. 12. Chemical composition and pH of the pore solution of paste #$P_{2.58}$ (w/c = 1, Mg/*P* = 1, $[B(OH)_3]_{initial}$ = 417 mmol/L).

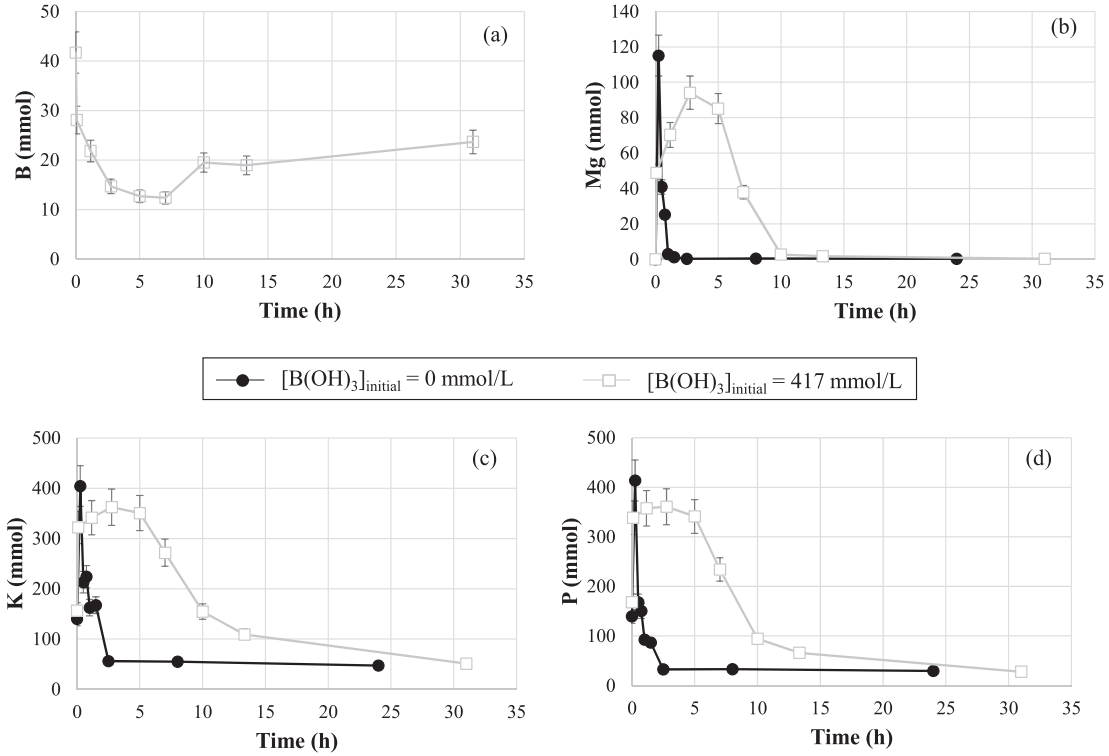

Fig. 13. Evolution of the molar numbers of B (a), Mg (b), K (c) and P (d) in the pore solutions of paste #P_0 ($[B(OH)_3]_{initial}$ = 0 mol/L) and paste #$P_{2.58}$ ($[B(OH)_3]_{initial}$ = 417 mmol/L) over time (initial composition: 100 g of cement + 100 g of water).

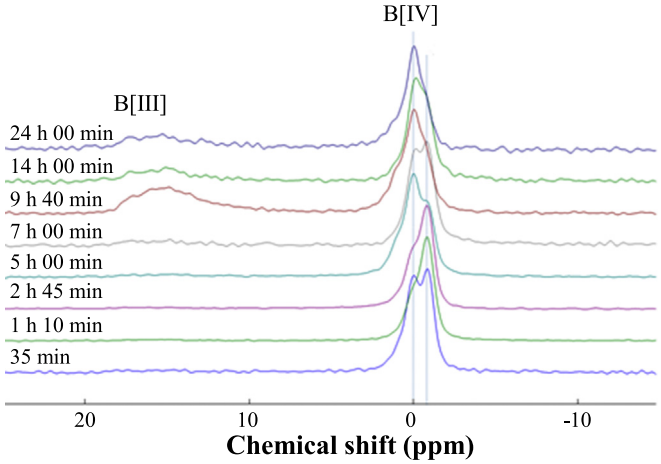

Fig. 14. ^{11}B MAS NMR spectra of the solid fraction of paste #$P_{2.58}$ comprising MgO, KH_2PO_4, $B(OH)_3$ and H_2O (w/c = 1, Mg/*P* = 1, $[B(OH)_3]_{initial}$ = 417 mmol/L) at different stages of hydration (35 min to 1 day).

onwards, which confirms that a portion of the boron was insolubilized. Two main peaks were observed with chemical shifts in the range [18; 12 ppm] and [1; −2 ppm], which are characteristic of three- and four-fold coordinated boron atoms respectively. ^{11}B (natural abundance 80.22%) is a quadrupolar nucleus (its nuclear spin is 3/2). The amplitude of the quadrupolar interaction it experiences depends strongly on the asymmetry of the local environment. The second-order terms of the interactions are only partially averaged by MAS, and this results in broadened lineshapes such as those in Fig. 14 assigned to B[III] sites [72,73]. The quadrupolar coupling is weaker for the more symmetric tetrahedral B[IV] sites and the corresponding signals are nearly Gaussian [74]. Trigonal boron was observed in the samples aged for 9 h 40 min and longer, once the paste had set, but tetragonal boron was detected in all the samples. The shoulders in the B[IV] lineshapes indicate that there are several B[IV] sites. The experimental spectra were fitted using five peaks, one for trigonal boron, and four for tetrahedral boron sites. Their chemical shift and full-width at half maximum were kept nearly constant for all the fits (Fig. 15-a, Table 3). This analysis shows that the populations of the five boron sites changed during the hydration process (Fig. 15-b). In particular, the fraction of boron with a chemical shift of −0.87 ± 0.04 ppm (contribution 4 in Table 3) seemed to decrease after 2 h 45 min. The release of boron into the pore solution might therefore follow the destabilization of an amorphous mineral containing four-fold coordinated boron.

3.2.4.2. ^{11}B – ^{31}P MAS-NMR spectroscopy. In addition, $^{31}P/^{11}B$ D-HMQC correlation experiments were performed on the solid fraction of paste #$P_{2.58}$ aged for 2 h 45 min (before the setting) and 9 h 40 min (just after the setting) using the D-HMQC technique. The 2D correlation maps obtained are shown in Fig. 16. In the 2 h 45 min-old sample, the B [IV] sites are located close to orthophosphate moieties. Even if spatial proximity does not necessarily prove that there is a chemical connectivity between the groups, in many cases, the proximity highlighted by the D-HMQC method is considered as selective enough to be representative of chemical bonds [59]. This suggests that the amorphous compound that precipitates during the first stages of hydration contains both phosphate and borate moieties. Elbers et al. [75] have determined the chemical shift of four-fold coordinated boron depending on its connectivity with orthophosphate groups in Ag_2O-B_2O_3-P_2O_5 glass: δ = [0.5; −0.1 ppm] for BO_4^{2-} groups linked via a bridging oxygen to a single P group (referred as $B_{(1P)}^4$); δ = [−0.4; −1.0 ppm] for BO_4^{2-} groups involved in two B-O-P links ($B_{(2P)}^4$); and δ = [−2.3; −2.8 ppm] for BO_4^{2-} groups involved in three B-O-P links ($B_{(3P)}^4$). The two main resonances observed at δ = −0.87 ppm and δ = −0.01 ppm in the spectra recorded for paste #$P_{2.58}$ at an early age can thus be assigned to BO_4^{2-} units respectively connected to two ($B_{(2P)}^4$) and one ($B_{(1P)}^4$) orthophosphate unit(s). The 2D spectrum of the older paste sample (9 h 40 min of hydration), still shows a correlation between P and BO_4 species, but none between P and BO_3 groups. There

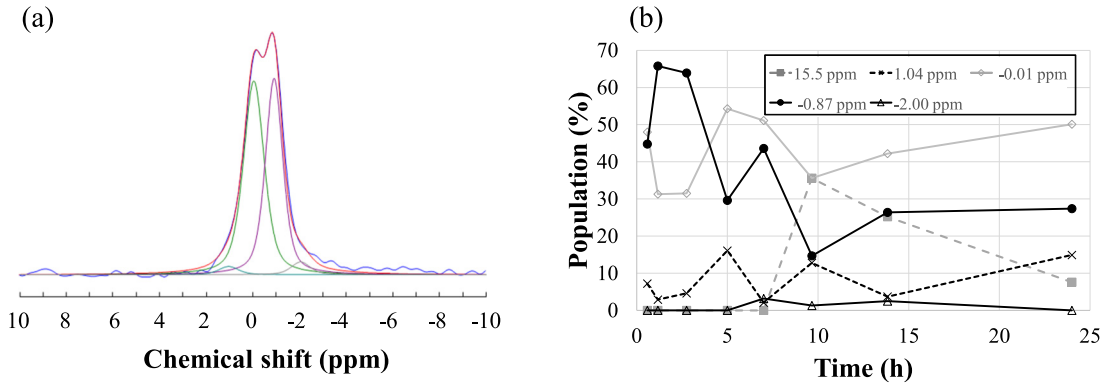

Fig. 15. Fitting of the ^{11}B-MAS NMR spectra. (a) Fit using four components of the lineshape assigned to tetracoordinated boron in the 7 h-old sample (blue line: experiment, red line: fit). (b) Populations of three- and fourfold coordinated boron atoms in the solid fraction of paste #$P_{2.58}$ at different stages of hydration. (For interpretation of the references to colour in this figure legend, the reader is referred to the web version of this article.)

Table 3
^{11}B NMR lineshape fitting parameters.

Time	Contribution 1			Contribution 2			Contribution 3			Contribution 4			Contribution 5		
	δ1	FWMH	Population	δ2	FWMH	Population	δ3	FWMH	Population	δ4	FWMH	Population	δ5	FWMH	Population
	ppm	kHz	%	ppm	kHz	%	ppm	kHz	%	ppm	kHz	%	ppm	kHz	%
35 min	15.50	0.00	0	1.00	1.00	7.2	0.02	1.00	48	−0.91	0.88	44.8	−2.00	0.00	0
1 h 10 min	15.50	0.00	0	1.00	1.00	2.9	0.00	1.03	31.3	−0.87	0.92	65.8	−2.00	0.00	0
2 h 45 min	15.50	0.00	0	1.02	1.01	4.6	0.03	1.01	31.5	−0.86	0.96	63.9	−2.00	0.00	0
5 h	15.50	0.00	0	1.03	1.06	16.1	0.02	1.04	54.3	−0.91	0.94	29.6	−2.00	0.00	0
7 h	15.50	0.00	0	1.04	1.04	2.1	−0.04	1.05	51.1	−0.91	0.88	43.6	−2.05	0.97	3.2
9 h 40 min	15.50	4.00	35.6	1.06	1.08	12.8	−0.01	1.06	35.6	−0.86	0.92	14.7	−2.00	0.95	1.3
13 h 50 min	15.50	4.50	25.2	1.05	1.00	3.7	−0.06	1.05	42.2	−0.86	0.97	26.4	−2.00	0.95	2.5
24 h	15.50	3.50	7.6	1.06	1.20	14.9	−0.03	1.05	50.1	−0.87	0.90	27.4	−2.00	0.00	0

are also no tetragonal boron sites in the vicinity of orthophosphate groups in K-struvite. There are two possible explanations for the presence of trigonal boron in the paste after setting: (*i*) $B(OH)_3$ may be adsorbed onto residual MgO or some of the hydrates, and (*ii*) a magnesium borate or potassium borate phase without phosphates may precipitate. In their review of hydrated borate minerals, Christ and Clark [76] list twelve minerals containing trigonal boron as well as magnesium and/or potassium.

3.3. Discussion about the retardation effect of boric acid

3.3.1. Does boric acid retard the dissolution of MgO or the precipitation of hydrates?

Our results show that the initial dissolution rates of MgO or KH_2PO_4 are not substantially altered by the presence of boric acid in water. However, the subsequent stages of hydration proceeded more slowly, the more so the higher the concentration of boric acid was. The question then is whether boric acid retarded the dissolution of the reactants or the precipitation of the products. Nicoleau et al. [77] have recently underlined the importance of some concepts of heterogeneous kinetics which are relevant for investigations of the hydration of mineral A into mineral B by dissolution/precipitation. The driving force for the reactions is the deviation from equilibrium: $\mu_i^A > \mu_i^{solution} > \mu_i^B$, where μ_i is the chemical potential of species *i* common to A and B. The equilibrium state is the solubility of solid in solution. A deviation from equilibrium is called undersaturation for the dissolution reaction, and supersaturation for the precipitation reaction. The lower the undersaturation is with respect to solid A, the slower it dissolves. The lower the supersaturation is with respect to solid B, the slower it precipitates. The rates of dissolution and precipitation are coupled when solids A and B contain common species. Indeed, the precipitation of solid B increases the level of undersaturation with respect to solid A and inversely, the dissolution of solid A increases the level of supersaturation with respect to solid B. The evolution of the composition

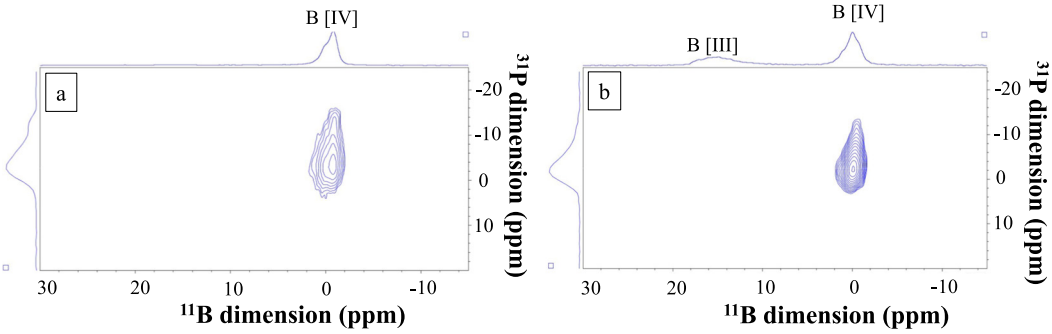

Fig. 16. ^{31}P/^{11}B correlation NMR spectra of the solid fraction of paste #$P_{2.58}$ aged for 2 h 45 min (a) and 9 h 40 min (b).

during the transformation of A into B defines the kinetic pathway, which can be plotted as an ion activity product vs. time diagram, and which always remains within the limits defined by the solubility products of A and B. If the kinetic pathway is close to the solubility product of A and far from that of B, the transformation is driven by the precipitation of B. On the contrary, if the pathway is close to the solubility product of B and far from that of A, the transformation is driven by the dissolution of A. Based on these considerations, we calculated the evolution over time of the ion activity products associated with the main reactions involved in MKPC hydration (Eqs. (1)–(4)).

$$MgO + 2\,H^+ \rightarrow Mg^{2+} + H_2O$$
$$\Pi_1 = (Mg^{2+})/(H^+)^2 \quad \text{(Eq. 1)}$$

$$MgHPO_4{\cdot}7H_2O \rightarrow Mg^{2+} + HPO_4^{2-} + 7\,H_2O$$
$$\Pi_2 = (Mg^{2+})(HPO_4^{2-}) \quad \text{(Eq. 2)}$$

$$Mg_2KH(PO_4)_2{\cdot}15H_2O + H^+ \rightarrow 2Mg^{2+} + K^+ + 2HPO_4^{2-} + 15\,H_2O$$
$$\Pi_3 = (Mg^{2+})^2(K^+)(HPO_4^{2-})^2/(H^+) \quad \text{(Eq. 3)}$$

$$MgKPO_4{\cdot}6H_2O + H^+ \rightarrow Mg^{2+} + K^+ + HPO_4^{2-} + 6\,H_2O$$
$$\Pi_4 = (Mg^{2+})(K^+)(HPO_4^{2-})/(H^+) \quad \text{(Eq. 4)}$$

The activities were calculated using the software Chess [78] and its thermodynamic database was supplemented with aqueous boron-containing species and phosphate minerals [42,79]. The solubility products taken for $MgHPO_4{\cdot}7H_2O$ and $Mg_2KH(PO_4)_2{\cdot}15H_2O$ were those reported by Chau et al. [40]. The input data were the experimentally measured pHs and compositions (total concentrations of Mg, P, B and K) of the pore solutions of pastes $\#P_0$ and $\#P_{2.58}$ at different hydration times. Fig. 17 compares the evolution of the activity products in the absence versus in the presence of boric acid. The two pastes were always undersaturated with respect to MgO and saturated or supersaturated with respect to $MgHPO_4{\cdot}7H_2O$, $Mg_2KH(PO_4)_2{\cdot}15H_2O$ and $MgKPO_4{\cdot}6H_2O$.

In paste $\#P_0$ (without boric acid), from 0 to ~1.5 h, the kinetic pathway moves closer to the solubility product of MgO, and away from those of the cement hydrates. The kinetics of the system is thus controlled by the precipitation of hydrates rather than by the dissolution of MgO at the beginning of the hydration process. Then, after 1.5 h, the reverse behavior is observed: the kinetic pathway moves away from the solubility product of MgO, and closer to those of the hydrates. The system is thus governed by the dissolution of MgO during the period when K-struvite is the main product formed. The trends are similar in paste $\#P_{2.58}$ (with boric acid): the system is initially driven by the precipitation of hydrates (from 0 to 5 h), and then by the dissolution of MgO. The main difference is that the two periods last much longer in the presence of boric acid.

3.3.2. *What are the processes involved in the retardation effect of boric acid?*

As introduced in Section 1, several hypotheses have been put forward in the literature to explain the retardation effect of boric acid. The adsorption of boric acid or the precipitation of a coating layer of a borate mineral on the surface of MgO may occur and may slow down the dissolution of MgO, but not during the first stage of the hydration process (which is governed by the precipitation rate of hydrates). Two further possible explanations remain: (*i*) the precipitation of lünebergite [49,50] or of an amorphous borate mineral [51] which may fix the pH and concentrations and thus create conditions that slow down the precipitation of hydrates, and (*ii*) the stabilization of magnesium in solution either by complexation, as postulated by Soudée [50], or by outbalancing the negative charges resulting from the formation of borates or polyborates when the pH increases [42]. These two hypotheses can be reexamined in light of the results obtained in this study.

3.3.2.1. Precipitation of a borate mineral. A boron-containing phase did precipitate during the early stages of the hydration process and consumed some of the boron from the pore solution. This phase was not detected by XRD, meaning that it was amorphous or of low crystallinity. It degraded below 100 °C and thus must have contained loosely bound water. A possible assignment that would fit with these observations is poorly crystallized lünebergite ($Mg_3B_2(PO_4)_2(OH)_6{\cdot}6H_2O$). Crystalline lünebergite was synthesized following the protocol given in Table 2 and was characterized by ^{31}P and ^{11}B MAS-NMR. The ^{31}P spectrum contains one peak at a chemical shift of $\delta = -2.7$ ppm (Fig. 18-a). The phosphorus is thus in just one (orthophosphate) chemical environment, which is consistent with the structure established by Sengupta et al. [80]. Similarly, the ^{11}B spectrum contains one peak at a chemical shift of 0.47 ppm (Fig. 18-b), characteristic of tetragonal boron bound to one PO_4 group ($B_{(1P)}^4$) [75]. This agrees well again with the structure of lünebergite. The $^{31}P/^{11}B$ correlation maps measured for the $\#P_{2.58}$ sample aged for 2 h 45 min (Fig. 16) show a broad correlation peak over a chemical shift range ($3 > \delta\,(^{31}P) > -12$ ppm; $2 > \delta(^{11}B) > -1.5$ ppm) that includes the values measured for lünebergite. Nevertheless, if this phase formed, it must have been accompanied by the precipitation of

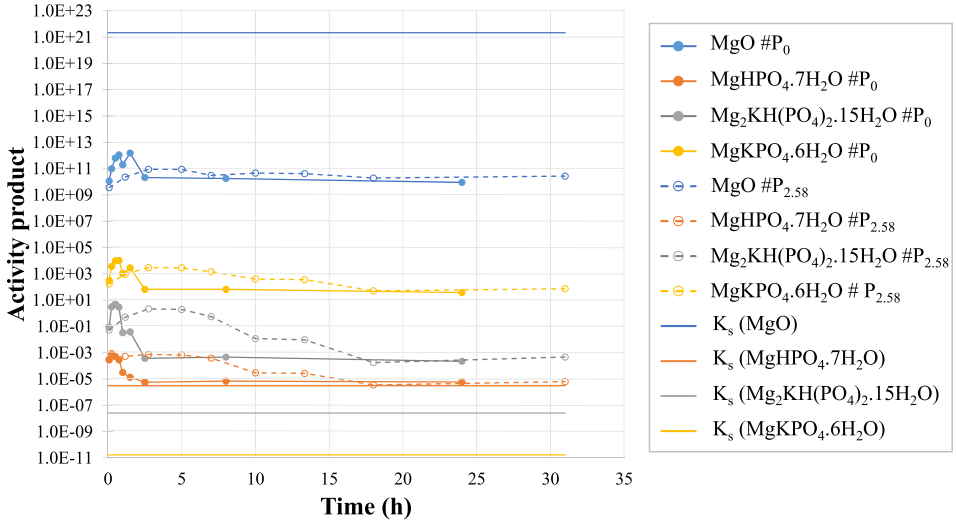

Fig. 17. Evolution of the activity products of MgO (Eq. 1), $MgHPO_4{\cdot}7H_2O$ (Eq. 2), $Mg_2KH(PO_4)_2{\cdot}15H_2O$ (Eq. 3) and $MgKPO_4{\cdot}6H_2O$ (Eq. 4) in the pore solution of pastes $\#P_0$ (full lines – without boric acid) and $\#P_{2.58}$ (dotted lines – with boric acid). Comparison with the solubility products of these phases.

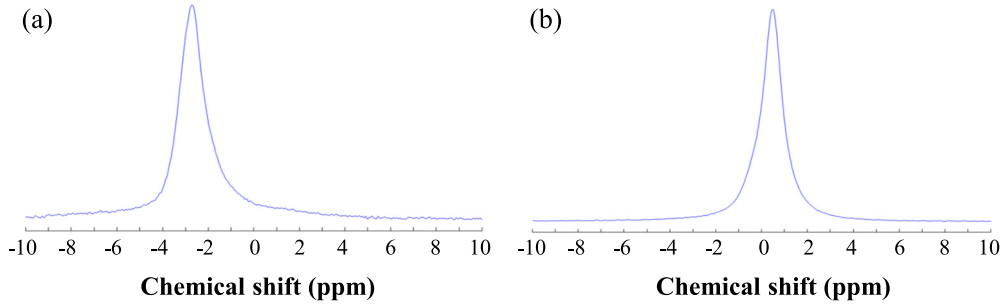

Fig. 18. Characterization of lünebergite ($Mg_3B_2(PO_4)_2(OH)_6{\cdot}6H_2O$) by MAS-NMR spectroscopy. (a) ^{31}P spectrum; (b) ^{11}B spectrum.

other boron-containing minerals. The ^{11}B MAS-NMR spectra of paste #$P_{2.58}$ (Fig. 14) indicate indeed that there are at least two tetragonal boron sites, which are connected to one ($B_{(1P)}^4$) or 2 ($B_{(2P)}^4$) orthophosphate groups. The borated mineral(s) precipitating initially is (are) then partly destabilized (Fig. 14, Table 3). A change in the boron environment in the solid phase occurs and some boron is released into the solution while hydration accelerates.

3.3.2.2. Stabilization of magnesium in solution. The magnesium released into the solution was consumed more slowly in the presence of boric acid (Fig. 13). A possible explanation might be that the magnesium is stabilized by the formation of a complex such as $MgB(OH)_4^+$. The speciation of the pore solution of paste #$P_{2.58}$ was calculated at 2 h 45 min using the software Chess and its enriched database. This is the time at which the total magnesium concentration reaches its maximum. The calculated $MgB(OH)_4^+$ concentration is negligible (0.55 µmol/L), indicating that this complex does not play a key role. The second possible explanation, based on the evolution of the boron speciation with pH, is therefore more likely. Polyborate ions ($B_3O_3(OH)_4^-$, $B_4O_5(OH)_4^{2-}$, $B_5O_6(OH)_4^-$) form when the pH increases above 6 [81]. To maintain electrical balance, their negative charges have to be compensated by cations in solution (Mg^{2+} and K^+, as shown in Fig. 13).

3.3.3. Influence of the w/c ratio on the retardation by boric acid

The results obtained for paste #$P_{2.58}$ (w/c = 1, [$B(OH)_3]_{initial}$ = 417 mmol/L) can be compared to those previously reported for a diluted suspension (w/c = 100, [$B(OH)_3]_{initial}$ = 4.17 mmol/L) [42]. Note that the $B(OH)_3$-to-cement ratio is the same in both cases. MKPC hydration is retarded in the paste and in the diluted suspension, but the more so in the paste: the time at which the electrical conductivity reached its second maximum was postponed by 8 h, versus < 1 h in the diluted suspension. The speciation of boron differed between the two systems. In the paste, boron partly precipitated during the early stages of hydration. In the suspension, the solution never became saturated with respect to borate minerals and boron remained dissolved in the solution. This comparison suggests that MKPC hydration can be delayed by at least two mechanisms, one involving boron dissolved in the solution, the other involving boron precipitated as a phosphate mineral. The latter seems to have a stronger retardation effect than the former.

4. Conclusion

The following conclusions can be drawn from this work on the hydration of MKPC in a paste and its retardation by boric acid.

1. The hydration of MKPC is a dissolution – precipitation process. The main hydrate is K-struvite ($MgKPO_4{\cdot}6H_2O$). Its precipitation is preceded by that of two transient phases: phosphorösslerite ($MgHPO_4{\cdot}7H_2O$) and $Mg_2KH(PO_4)_2.15H_2O$. Newberyite, a degradation product of phosphorösslerite, forms after the hydration stop during the storage of the samples rather than during the hydration process itself.
2. The hydration of MKPC in a paste (w/c = 1) follows a multi-step process similar to the one previously described for a suspension (w/c = 100). There are two differences however.

– In addition to phosphorösslerite ($MgHPO_4{\cdot}7H_2O$) and $Mg_2KH(PO_4)_2{\cdot}15H_2O$, our results suggest that small amounts of other phosphate minerals form transiently.
– Cattiite ($Mg_3(PO_4)_2{\cdot}22H_2O$), one of the end-products in the suspension, is not observed in the paste and the final pH of the pore solution is reduced by 1.6 in the paste (pH 8.4 instead of 10).

3. Boric acid retards the hydration of MKPC and partly precipitates at the beginning of the process. The borate mineral(s) contain(s) fourfold coordinated boron, with two main chemical environments, namely BO_4^{2-} units connected to one and two orthophosphate moieties. While the precipitation of poorly crystallized lünebergite ($Mg_3B_2(PO_4)_2(OH)_6{\cdot}6H_2O$) cannot be ruled out, our data show that another mineral containing tetragonal boron connected to two orthophosphate groups must also form. The compound(s) that precipitate(s) initially evolve(s) during hydration and become(s) partially destabilized, leading to a release of boron into the solution and a second increase in pH. In the same time, the hydration process accelerates.
4. Different boron species form in the paste (w/c = 1) and in the suspension (w/c = 100). In the suspension indeed, boron remains dissolved in the pore solution during the whole hydration period.
5. The hydration of a MKPC paste is driven first by the precipitation of hydrates, and then by the dissolution of MgO. This is also what happens in the presence of boric acid, but much more slowly. Several processes may contribute to this retardation: the initially precipitated mineral(s) containing borates and phosphates may create pH and concentrations conditions in the solution that delay the precipitation of hydrates. In addition, cations (Mg^{2+} and K^+) may be stabilized in the solution to counterbalance the negative charges that result from the formation of polyborates at pHs higher than 6. Finally, the dissolution of MgO might be slowed down by the adsorption of boric acid or by the precipitation of a dense coating of hydrates.

Acknowledgements

This work received financial support from the interdisciplinary NEEDS project (involving ANDRA, CNRS, EDF, AREVA, CEA and IRSN) and from IR RMN THC FR3050. The authors thank Bertrand Revel (Centre commun de mesures RMN, Lille 1 University of Science and Technology) for his help with the NMR experiments.

Appendix A

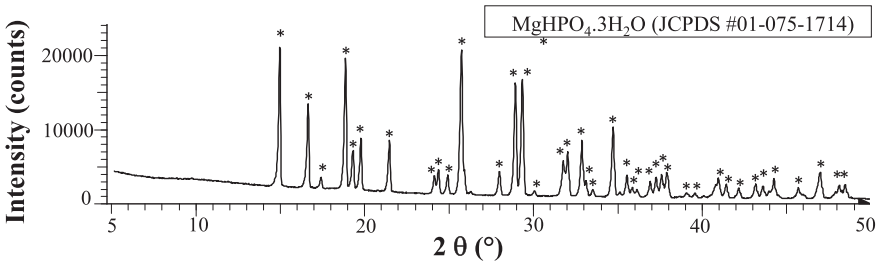

Fig. A.1. XRD pattern of newberyite ($MgHPO_4{\cdot}3H_2O$) synthesized as described in Table 2.

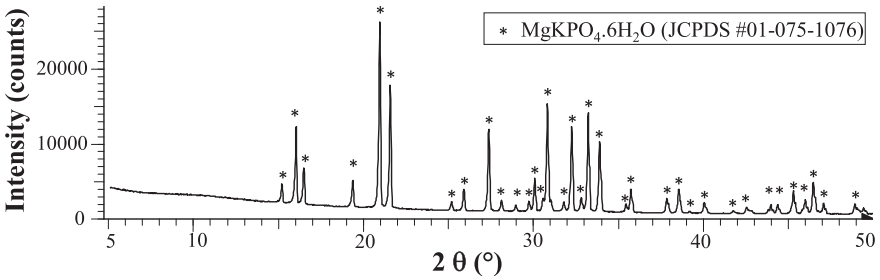

Fig. A.2. XRD pattern of K-struvite ($MgKPO_4{\cdot}6H_2O$) synthesized as described in Table 2.

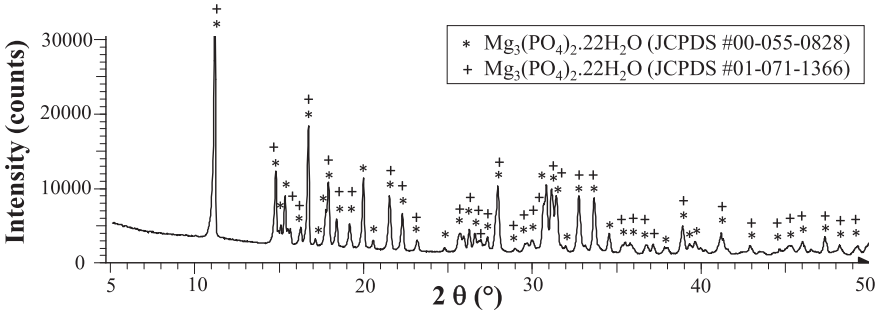

Fig. A.3. XRD pattern of cattiite ($Mg_3(PO_4)_2{\cdot}22H_2O$) synthesized as described in Table 2. The diffraction pattern of the product synthesized in this work is very similar to that of a natural cattiite specimen from Zhelezny iron mine, Kovdor, Russia (JCPDS file # 00-055-0828), except that it contains two additional peaks at $2\theta = 27.0^{\circ}$ and 37.2°. These reflections are however reported for a synthetic cattiite sample in JCPDS file # 01-071-1366.

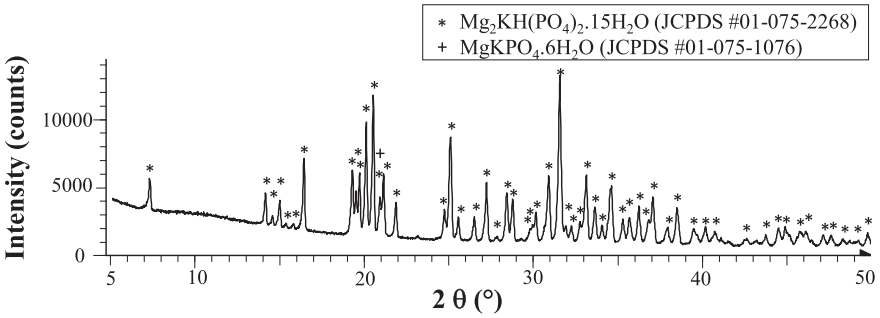

Fig. A.4. XRD pattern of $Mg_2KH(PO_4)_2{\cdot}15H_2O$ synthesized as described in Table 2. Traces of K-struvite might contribute to the reflection at $2\theta = 21.9^{\circ}$.

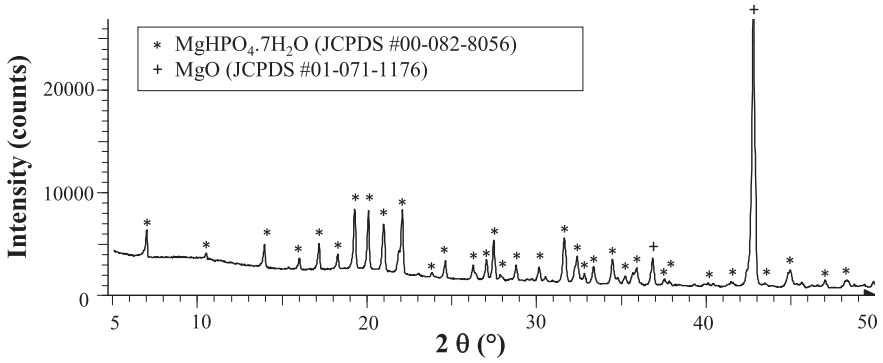

Fig. A.5. XRD pattern of phosphorösslerite ($MgHPO_4{\cdot}7H_2O$) and periclase (MgO) obtained as described in Table 2.

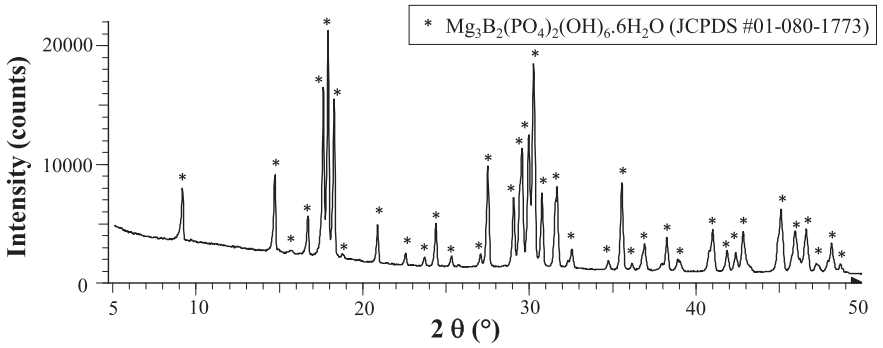

Fig. A.6. XRD pattern of lünebergite ($Mg_3B_2(PO_4)_2(OH)_6{\cdot}6H_2O$) synthesized as described in Table 2.

References

[1] E. Weill, J. Bradik, Magnesium phosphate cement systems, US Patent n° 4 756 762 (1988).

[2] I. Odler, Special Inorganic Cements, Modern Concrete Technology Series, Taylor & Francis, London, 2000, pp. 216–224.

[3] J. Bensted, Rapid setting magnesium phosphate cement for quick repair of concrete pavements - characterization and durability aspects – discussion, Cem. Concr. Res. 24 (1994) 595–596.

[4] Q. Yang, B. Zhu, X. Wu, Characteristics and durability test of magnesium phosphate cement-based material for rapid repair of concrete, Mater. Struct. 33 (2000) 229–234.

[5] F. Qiao, C.K. Chau, Z. Li, Property evaluation of magnesium phosphate cement mortar as patch repair material, Constr. Build. Mater. 24 (2010) 695–700.

[6] G. Mestres, M.P. Ginebra, Novel magnesium phosphate cements with high early strength and antibacterial properties, Acta Biomater. 7 (2011) 1853–1861.

[7] G. Mestres, M. Abdolhosseini, W. Bowles, S.-H. Huang, C. Aparicio, S.-U. Gorr, M.-P. Ginebra, Antimicrobial properties and dentin bonding strength of magnesium phosphate cements, Acta Biomater. 9 (2013) 8384–8393.

[8] H. Zhou, A.K. Agarwal, V.K. Goel, S.B. Bhaduri, Microwave assisted preparation of magnesium phosphate cement (MPC) for orthopedic applications: a novel solution to the exothermicity problem, Mater. Sci. Eng. C 33 (2013) 4288–4294.

[9] I. Buj, J. Torras, M. Rovira, J. de Pablo, Leaching behaviour of magnesium phosphate cements containing high quantities of heavy metals, J. Hazard. Mater. 175 (2010) 789–794.

[10] I. Buj, J. Torras, D. Casellas, M. Rovira, J. de Pablo, Effect of heavy metals and water content on the strength of magnesium phosphate cements, J. Hazard. Mater. 170 (2009) 345–350.

[11] S.C. Zhen, X.H. Donh, P.N. Nkrumah, Y. Su, D.K. Zhou, Effects of fly ash on the solidification/stabilization of heavy metals with magnesium phosphate cement, Int. J. Earth Sci. Eng. 7 (2014) 1274–1279.

[12] J.R. Wang, B.G. Ma, X.G. Li, H.N. Li, Z. Tian, The solidification and hydration products of magnesium phosphate cement with Pb^{2+}, Zn^{2+} and Cu^{2+}, J. Funct. Mater. 45 (2014) 05060–05064.

[13] Y. Su, J. Yang, S. Zhen, N. Lin, Y. Zhou, Solidification/stabilization of simulated cadmium-contaminated wastes with magnesium potassium phosphate cement, Environ. Eng. Res. 21 (2016) 15–21.

[14] Y. Du, M.L. Wei, K.R. Reddy, F. Jin, H.L. Wu, Z.B. Liu, New phosphate-based binder for stabilization of soils contaminated with heavy metals: leaching, strength and microstructure characterization, J. Environ. Manag. 146 (2014) 179–188.

[15] X. Xu, J. Yang, Y. Gu, Properties of magnesium potassium phosphate cement containing heavy metal Pb, J. Building Mater. 19 (2016) 29–34.

[16] D. Véras Ribeiro, M.R. Morelli, Influence of the addition of grinding dust to a magnesium phosphate cement matrix, Constr. Build. Mater. 23 (2009) 3094–3102.

[17] A.S. Wagh, D. Singh, S.Y. Jeong, R.V. Strain, Ceramicrete stabilization of low-level mixed wastes, a complete story, Proc. 18th Annual DOE Low-Level Radioactive Waste Management Conference, Salt Lake City, UT, USA, 20–22 May, 1997.

[18] A. Covill, N.C. Hyatt, J. Hill, N.C. Collier, Development of magnesium phosphate cements for radioactive waste, Adv. Appl. Ceram. 110 (2011) 151–156.

[19] C.A. Langton, D.B. Stefanko, M.G. Serrato, J.K. Blankenship, W.B. Griffin, J.T. Waymer, D. Matheny, D. Singh, Use of cementitious materials for SRS reactor facility in-situ decommissioning, Proc. Waste Management (WM'11) 2011 Conference, Phoenix, USA, 2011.

[20] D. Singh, A.S. Wagh, M. Tlustochowicz, S.Y. Jeong, Phosphate ceramic process for macroencapsulation and stabilization of low-level debris wastes, Waste Manag. 18 (1998) 135–143.

[21] C. Cau Dit, D. Coumes, H. Lambertin, P. Lahalle, C. Antonucci, S. Delpech Cannes, Selection of a mineral binder with potentialities for the stabilization/solidification of aluminum metal, J. Nucl. Mater. 453 (2014) 31–40.

[22] A.S. Wagh, S.Y. Sayenko, V.A. Shkuropatenko, R.V. Tarasov, M.P. Dykiy, Y.O. Svitlychniy, V.D. Virych, E.A. Ulybkina, Experimental study on caesium immobilization in struvite structures, J. Hazard. Mater. 302 (2016) 241–249.

[23] E. Soudée, J. Pera, Mechanism of setting reaction in magnesia-phosphate cements, Cem. Concr. Res. 30 (2000) 315–321.

[24] A.S. Wagh, Chemically Bonded Phosphate Ceramics, Elsevier, Amsterdam, 2004, pp. 264–267.

[25] D. Hou, H. Yan, J. Zhang, P. Wang, Z. Li, Experimental and computational investigation of magnesium phosphate cement mortar, Constr. Build. Mater. 112 (2016) 331–342.

[26] N. Yang, C. Shi, J. Yang, Y. Chang, Research progresses in magnesium phosphate cement-based materials (review), J. Mater. Civ. Eng. 26 (2014) (article n°04014071).

[27] B. Xu, H. Ma, Z. Li, Influence of magnesia-to-phosphate molar ratio on microstructures, mechanical properties and thermal conductivity of magnesium potassium phosphate cement paste with large water-to-solid ratio, Cem. Concr. Res. 68 (2015) 1–9.

[28] Z.Q. Qi, H.T. Wang, J.H. Ding, S.H. Zhang, Study on the drying shrinkage property of magnesium phosphate cement, Mater. Sci. Forum 852 (2016) 1468–1472.

[29] M. Le Rouzic, T. Chaussadent, L. Stefan, M. Saillio, On the influence of Mg/P ratio on the properties and durability of magnesium potassium phosphate cement pastes, Cem. Concr. Res. 96 (2017) 27–41.

[30] A.J. Wang, Z.L. Yuan, J. Zhang, L.T. Liu, J.M. Li, Z. Liu, Effect of raw material ratios on the compressive strength of magnesium potassium phosphate chemically bonded ceramics, Mater. Sci. Eng. C 33 (2013) 5058–5063.

[31] R.Q. Liu, D.Q. Chen, T.B. Hou, Study on preparation and setting time of magnesium potassium phosphate cement, Adv. Mater. Res. 1049 (2014) 251–255.

[32] H. Ma, B. Xu, J. Liu, H. Pei, Z. Li, Effects of water content, magnesia-to-phosphate molar ratio and age on pore structure, strength and permeability of magnesium potassium phosphate cement paste, Mater. Des. 64 (2014) 497–502.

[33] Y. Li, J. Sun, B. Chen, Experimental study of magnesia and M/P ratio influencing properties of magnesium phosphate cement, Constr. Build. Mater. 65 (2014) 177–183.
[34] H. Ma, B. Xu, Potential to design magnesium potassium phosphate cement paste based on an optimal magnesia-to-phosphate ratio, Mater. Des. 118 (2017) 81–88.
[35] M. Xue, H. Wang, X. Xiao, J. Cao, Influence of m(P)/m(M) mass ratio on properties of magnesium phosphate cement and its mechanism analysis, J. Funct. Mater. 46 (2015) 23090–23095.
[36] P.K. Mehta, Magnesium oxide additive for producing self-stress in mass concrete, Proc. 7th Intern. Congress on the Chemistry of Cement, Paris, France, 3 1980, pp. 6–9.
[37] A.H. White, Volume changes of Portland cement as affected by chemical composition and ageing, Proc. Am. Soc. Test. Mater. 28 (1928) 398–431.
[38] B. Xu, H. Ma, H. Shao, Z. Li, B. Lothenbach, Influence of fly ash on compressive strength and micro-characteristics of magnesium potassium phosphate cement mortars, Cem. Concr. Res. 99 (2017) 86–94.
[39] B. Xu, B. Lothenbach, A. Leemann, F. Winnefeld, Reaction mechanism of magnesium potassium phosphate cement with high magnesium-to-phosphate ratio, Cem. Concr. Res. 108 (2018) 140–151.
[40] C.K. Chau, F. Qiao, Z. Li, Potentiometric study of the formation of magnesium potassium phosphate hexahydrate, J. Mater. Civ. Eng. 24 (2012) 586–591.
[41] S. Zhen, X. Dong, G. Appiah-Sefah, M. Pan, D. Zhou, Analysis of changes in hydration products during solidification/stabilization process of heavy metals in the presence of magnesium potassium phosphate cement, J. Appl. Sci. Eng. 17 (2014) 413–421.
[42] H. Lahalle, C. Cau Dit Coumes, A. Mesbah, D. Lambertin, C. Cannes, S. Delpech, S. Gauffinet, Investigation of magnesium phosphate cement hydration in diluted suspension and its retardation by boric acid, Cem. Concr. Res. 87 (2016) 77–86.
[43] A. Viani, M. Peréz-Esteban, S. Pollastri, A.F. Gualtieri, In situ synchrtron powder diffraction study of the setting reaction kinetics of magnesium-potassium phosphate cements, Cem. Concr. Res. 79 (2016) 344–352.
[44] M. Le Rouzic, T. Chaussadent, G. Platret, L. Stefan, Mechanisms of k-struvite formation in magnesium phosphate cements, Cem. Concr. Res. 91 (2017) 117–122.
[45] Q. Yang, X. Wu, Factors influencing properties of phosphate cement-based binder for rapid repair of concrete, Cem. Concr. Res. 29 (1999) 389–396.
[46] J. Formosa, J.M. Chimenos, A.M. Lacasta, M. Niubó, Interaction between low-grade magnesium oxide and boric acid in chemically bonded phosphate ceramics formulation, Ceram. Int. 38 (2012) 2483–2493.
[47] X.Y. Duan, S.Z. Li, Z.Y. Lai, S.C. Mou, Q.L. Liao, Preparation of a multi-composite retarder and its effect on properties of magnesium phosphate cement, J. Wuhan Univer. Technol. 36 (2014) 20–25.
[48] D.A. Hall, R. Stevens, B.E. Jazairi, The effect of retarders on the microstructure and mechanical properties of magnesia–phosphate cement mortar, Cem. Concr. Res. 31 (2001) 455–465.
[49] A.S. Wagh, D. Singh, S.Y. Jeong, Stabilization of hazardous ash waste with new-beryite-rich chemically bonded magnesium phosphate ceramic, J. Mater. Res. 29 (1995) (35p).
[50] E. Soudée, Liants phospho-magnésiens: mécanisme de prise et durabilité (PhD thesis), INSA, Lyon, France, 1999 (in French).
[51] A.K. Sarkar, Phosphate cement-based fast setting binders, Ceram. Bull. 69 (1990) 234–238.
[52] L.J. Gardner, S.A. Bernal, S.A. Walling, C.L. Corkhill, J.L. Provis, N.C. Hyatt, Characterization of magnesium potassium phosphate cements blended with fly ash and ground granulated blast furnace slag, Cem. Concr. Res. 74 (2015) 78–87.
[53] D.R. Lide, CRC Handbook of Chemistry and Physics, 86th edition, CRC Press, Taylor & Francis, Boca Raton, Florida, 2005, pp. 4–79.
[54] J.B. Champenois, C. Cau Dit, A. Coumes, P. Poulesquen, D. Damidot Le Bescop, Beneficial use of a cell coupling rheometry, conductimetry and calorimetry to investigate the early age hydration of calcium sulfoaluminate cement, Rheol. Acta 52 (2013) 177–187.
[55] D. Massiot, F. Fayon, M. Capron, I. King, S. Le Calvé, B. Alonso, J.O. Durand, B. Bujoli, Z. Gan, G. Hoatson, Modelling one and two-dimensional solid-state NMR spectra, Magn. Reson. Chem. 40 (2002) 70–76.
[56] Z. Gan, $^{13}C/^{14}N$ heteronuclear multiple-quantum correlation with rotary resonance and REDOR dipolar recoupling, J. Magn. Reson. 184 (2007) 39–43.
[57] G. Tricot, O. Lafon, J. Trébosc, L. Delevoye, F. Méar, L. Montagne, J.P. Amoureux, Structural characterisation of phosphate materials: new insights into the spatial proximities between phosphorus and quadrupolar nuclei using the D-HMQC MAS NMR technique, Phys. Chem. Chem. Phys. 13 (2011) 16786–16794.
[58] A. Brinkmann, A.P.M. Kentgens, Proton-selective $^{17}O-H$ distance measurements in fast magic-angle-spinning solid-state NMR spectroscopy for the determination of hydrogen bond lengths, J. Am. Chem. Soc. 128 (2006) 14758–14759.
[59] G. Tricot, B. Raguenet, G. Silly, M. Ribes, A. Pradel, H. Eckert, P-O-B3 linkages in borophosphate glasses evidenced by high field $^{11}B/^{31}P$ correlation NMR, Chem. Commun. 51 (2015) 9284–9286.
[60] W.J. McCarter, P.N. Currant, The electrical response characteristics of setting cement paste, Mag. Concr. Res. 36 (1984) 42–49.
[61] L.J. Gardner, V. Lejeune, C.L. Corkhill, S.A. Bernal, J.L. Provis, M.C. Stennett, N.C. Hyatt, Evolution of phase assemblage of blended magnesium potassium phosphate cement binders at 200 °C and 1000 °C, Adv. Appl. Ceram. 114 (2015) 386–392.
[62] S.J. Kiehl, H.B. Hardt, The dissociation pressures of magnesium ammonium phosphate hexahydrate and sole related substances, J. Am. Chem. Soc. 7 (1993) 605–618.
[63] O.M. Friedrich, J. Robitsch, Phosphorrösslerit ($MgHPO_4{\cdot}7H_2O$) als Mineral aus dem Stülbau zu Schellgaden, Zentralbl. Miner. Geol. Palaontol. A (1939) 142–155 (in German).
[64] B.C. Sales, B.C. Chakoumakas, L.A. Boatner, J.O. Ramey, Structural evolution of the amorphous solids produced by heating crystalline $MgHPO_4.3H_2O$, J. Mater. Res. 7 (1992) 2646–2649.
[65] S. Hunger, H. Cho, J.T. Sims, D.L. Sparks, Direct speciation of phosphorous in alum-amended poultry litter: solid state ^{31}P NMR investigation, Environ. Sci. Technol. 38 (2004) 674–681.
[66] M.A. Aramendia, V. Borau, C. Jiminez, J.M. Marinas, F.J. Romero, J.R. Ruiz, XRD and solid-state NMR study of magnesium oxide – magnesium orthophosphate systems, J. Solid State Chem. 135 (1998) 96–102.
[67] N. Ma, A.A. Rouff, B.L. Philips, A ^{31}P NMR and TG/DSC-FTIR investigation of the influence of initial pH on phosphorus recovery as struvite, ACS Sustain. Chem. Eng. 2 (2014) 816–822.
[68] S. Takagi, M. Mathew, W.E. Brown, Water-rich hydrates. The structure of dimagnesium potassium hydrogen bis (arsenate) 15-hydrate and dimagnesium potassium hydrogen bis (phosphate) 15-hydrate, Acta Crystallogr. B 38 (1982) 44–50.
[69] M.G.W. Lockyer, D. Holland, R. Dupree, NMR investigation of the structure of some bioactive and related glasses, J. Non-Cryst. Solids 351 (2005) 207–219.
[70] I. Elgayar, A.E. Aliev, A.R. Boccaccini, R.G. Hill, Structural analysis of bioactive glasses, J. Non-Cryst. Solids 351 (2005) 173–183.
[71] A.V. Angeloupoulou, V. Montouillout, D. Massiot, G. Kordas, Study of the alkaline environment in mixed alkali compositions by multiple-quantum magic angle nuclear magnetic resonance (MQ-MAS NMR), J. Non-Cryst. Solids 354 (2008) 333–340.
[72] G.L. Turner, K.A. Smith, R.J. Kirkpatrick, E. Oldfield, Boron-11 nuclear magnetic resonance spectroscopic study of borate and borosilicate minerals and of a borosilicate glass, J. Magn. Reson. 67 (1986) 544–550.
[73] P.J. Bray, J.O. Edwards, J.G. O'Keefe, V.F. Ross, I. Tatsuzaki, Nuclear magnetic resonance studies of ^{11}B in crystalline borates, J. Chem. Phys. 35 (1961) 435–442.
[74] C. Gervais, F. Babonneau, High resolution solid state NMR investigation of various boron nitride preceramic precursors, J. Organomet. Chem. 657 (2002) 75–82.
[75] S. Elbers, W. Strojek, L. Koudelka, H. Eckert, Site connectivities in silver borophosphate glasses: new results from $^{11}B\{^{31}P\}$ and $^{31}P\{^{11}B\}$ rotational echo double resonance NMR spectroscopy, Solid State Nucl. Magn. Reson. 27 (2005) 65–76.
[76] C.L. Christ, J.R. Clark, A crystal-chemical classification of borate structures with emphasis on hydrated borates, Phys. Chem. Miner. 2 (1977) 59–87.
[77] L. Nicoleau, A. Nonat, A new view on the kinetics of tricalcium silicate hydration, Cem. Concr. Res. 86 (2016) 1–11.
[78] J. Van der Lee, Thermodynamic and Mathematical Concepts of CHESS, Technical Report LHM/RD/98/39, (1998) (99 pp.).
[79] T. Zhang, H. Chen, X. Li, Z. Zhu, Hydration behavior of magnesium potassium phosphate cement and stability analysis of its hydration products through thermodynamic modeling, Cem. Concr. Res. 98 (2017) 101–110.
[80] P. Sengupta, G. Swihart, R. Dimitrijevic, M. Hossain, The crystal structure of lünebergite, Am. Mineral. 76 (1991) 1400–1407.
[81] N. Ingri, Equilibrium studies of polyanions. 11. Polyborates in 3.0M NaBr, 3.0M LiBr and 3.0 M KBr, a comparison with data obtained in 3.0 M $NaClO_4$, Acta Chem. Scand. 17 (1963) 581–589.